Remote Sensing of Environment 226 (2019) 93–108

Contents lists available at ScienceDirect

Remote Sensing of Environment

journal homepage: www.elsevier.com/locate/rse

Retrieval of black carbon aerosol surface concentration using satellite remote sensing observations

Fangwen Bao[a,b,d], Tianhai Cheng[c,*], Ying Li[a,*], Xingfa Gu[c], Hong Guo[c], Yu Wu[c], Ying Wang[c], Jinhui Gao[a,d]

[a] Department of Ocean Sciences and Engineering, Southern University of Science and Technology, Shenzhen, China
[b] Department of Earth and Space Sciences, Southern University of Science and Technology, Shenzhen, China
[c] State Key Laboratory of Remote Sensing Science, Institute of Remote Sensing and Digital Earth of Chinese Academy of Sciences, Beijing, China
[d] School of Earth and Space Sciences, University of Science and Technology of China, Hefei, China

ARTICLE INFO

Keywords:
Black carbon concentration
Satellite remote sensing
Air pollution

ABSTRACT

As an important part of the anthropogenic aerosol, Black Carbon (BC) aerosols in the atmospheric environment have strong impacts on climate change. Recently, most remote sensing studies on aerosol components detection are limited to the inversion of aerosol optical properties, integration of chemistry models or in situ observations. In this paper, an algorithm based on Effective Medium Approximations (EMA) and statistically optimized aerosol inversion algorithm was integrated for retrieving the surface mass concentration of BC aerosols from satellite signals. The sensitivity analyses for the developed forward model proved that the volume fraction of vertical BC is sensitive to the satellite observations and significantly improved especially over bright surface targets or under polluted atmospheric conditions. By updating the forward model and retrieved parameters of the statistically optimized inversion algorithm, three cases of high aerosol loading days were retrieved from Polarization and Anisotropy of Reflectance for Atmospheric Sciences Coupled with Observations from a LiDAR (PARASOL) measurements, which shows a significant ability of BC aerosol detection. Additionally, the validation and closure studies of BC concentration retrievals also indicates an encouraging consistency with correlation (R) of 0.71, mean bias of 3.55, and root-mean-square error (RMSE) of 3.75 when compared against the in-situ observations over South Asia. The accuracy of the retrievals also demonstrates different trends under different levels of aerosol loadings, which shows a higher accuracy in biomass burning seasons (R = 0.75, RMSE = 4.04, Bias = 3.27) while exaggerates the results in the case of clear conditions (R = 0.47, RMSE = 4.83, Bias = 4.00). Finally, the uncertainties of three assumptions, including proposing uniform vertical profile for BC, neglecting light-absorbing aerosols and using spherical EMA models were discussed in our manuscript. The maximum standard deviations caused by these uncertainties on low BC aerosol volume fractions (f_{BC} < 1%) are 0.8%, 0.35% and 0.2% while these deviations will change to 0.25%, 0.05% and 1.5% respectively under higher BC fractions (f_{BC} > 5%). This conclusion confirmed that the proposed algorithm for BC surface concentration retrieval extends the application of satellite remote sensing in monitoring the extreme biomass burning pollution.

1. Introduction

Black Carbon (BC) in the atmospheric environment is an important part of anthropogenic aerosol, which emitted directly at the source from incomplete combustion processes such as fossil fuel and biomass burning. Bond et al. (2004) estimated the total current global emission of BC to be approximately 8 TgC yr^{-1}, with about 20% from biofuels, 40% from fossil fuels and 40% from open biomass burning. Additionally, BC in aerosol soot is the dominant absorber of visible solar radiation in the atmosphere, which plays a unique and important role on Earth's climate system (Bond et al., 2013; Ramanathan and Carmichael, 2008). It has been reported that the strong absorbing BC aerosol particles lead to atmospheric warming and offset the direct radiative impact of scattering aerosols by approximately 50–100% (Li et al., 2016; Takemura et al., 2005; Yang et al., 2017). This direct radiative forcing effect may be greater than most of greenhouse gases (e.g. methane) and equal to about half of that of carbon dioxide (Jacobson, 2001). In addition, the indirect effects of absorbing aerosols may also be responsible for the reduction of tropical cloudiness (Jones et al., 1994; Lohmann and Feichter, 2005) and explosive melt rates by

* Corresponding authors.
E-mail addresses: chength@radi.ac.cn (T. Cheng), liy66@sustech.edu.cn (Y. Li).

https://doi.org/10.1016/j.rse.2019.03.036
Received 21 September 2018; Received in revised form 26 February 2019; Accepted 25 March 2019
Available online 04 April 2019
0034-4257/ © 2019 Elsevier Inc. All rights reserved.

reducing the albedo of ice and snow in polar region (Flanner et al., 2007; Randerson et al., 2006).

Recently, several approaches have been proposed for evaluating BC concentrations in particulate matter. Sampling with Scanning Electron Microscopy (SEM) and Aerosol Mass Spectrometer (AMS) are the common approach for in-situ measurement of absorbing aerosols (DeCarlo et al., 2006; Ebert et al., 2002; Jayne et al., 2000; Jimenez et al., 2003). These in-situ observations provide accurate but limited spatial and temporal coverage results with 5%–10% error (0.05–50 μg/m3) (Khlystov et al., 1995; Ng et al., 2011). On the contrary, the simulation of aerosol concentrations via chemistry models coupled with transport models and general circulation models can provide global estimates (Ginoux et al., 2001). Typically, these chemical models are initialized by global or regional aerosol emission inventories and highly parameterized by basic meteorological environment (Bond et al., 1998; Streets et al., 2009). Thus, such dependent modeled inventories and meteorological input are extremely deviated from the real atmospheric environment and remain large uncertainties to the model output (Sato et al., 2003).

Apart from the sampling analysis and modeling simulation, the aerosol optical signals, which are determined by aerosol compositions, can be effectively obtained from in situ or space base remote sensing sensors. Thus, the studies of aerosol composition retrieval by using remote sensing signal have attracted the attention of many researchers. Recently, two aspects, including aerosol classification and aerosol component inversion, have been proposed in the most remote-sensing based aerosol studies. Dubovik et al. (2002) used aerosol optical information from the AErosol RObotics NETwork (AERONET) to classify aerosol types in several key locations. Moreover, combining the datasets of the AERONET sites, Omar et al. (2005) also proposed six globally distributed aerosol types by using the cluster analysis method. These classified methods can effectively identify the type of aerosols, which simply applied to the satellite aerosol model retrieval via Look-Up Table (LUT) method (Jackson et al., 2013; Lee et al., 2010).

However, these classification methods can only distinguish the dominant aerosol types and cannot quantify the aerosol concentrations. Aiming at resolving this problem, Schuster et al. (2005) takes the lead in putting forward an approach of retrieving three component concentration (BC and Ammonium Sulfate embedded in the water host) from AERONET imaginary refractive index. Following his work, many researchers extended the retrieval model by considering the additional spectral dependent restrictions (Arola et al., 2011; Dey et al., 2006), such as adding the aerosol Single Scattering Albedo (SSA) relationships via Mie scattering model (Wang et al., 2012; Wang et al., 2013), or proposing particle size distribution relationships through volume fraction ratio of fine to coarse mode (Xie et al., 2017).

Although the analyses of temporal change and regional comparison by using in situ BC concentration retrievals have been proposed by many researchers (Li et al., 2013; van Beelen et al., 2014), the single point results cannot express the spatial distribution especially over a region with non-synchronous ground observation and high aerosol loading (e.g. Ganges plain and North China Plain). Simultaneous observation produced by satellite remote sensing sensors can effectively monitor the aerosol optical properties over a large region but the satellite-based algorithm of the aerosol component concentration retrieval is still uncertain. Therefore, in this study, an expanded algorithm based on the effective medium approximation and the radiation transfer model for BC surface concentration retrieval is established at first. The sensitivity studies between volume fractions of BC aerosols and satellite radiative signals are highlighted in the following sections. The algorithm is applied to the Polarization and Anisotropy of Reflectance for Atmospheric Science coupled with Observations from a Lidar (PARASOL) microsatellite as well as the validation studies of BC concentration results are proposed with ground-based measurements. Finally, three aspects of uncertainty research were proposed for the future improvement.

2. Retrieval algorithm of BC surface concentration

2.1. Mixture morphology of aerosols

The specific mixture morphology of aerosol monomers in the atmosphere indicates a wide range of values, which is attributed to the internal or external physical properties of atmospheric particles (Liousse et al., 1993; Schuster et al., 2005). With strong absorption characteristics of BC aerosols, this mixture strategy would finally affect the optical properties of mixed aerosols and radiative signals of satellite sensors. Therefore, an accurate mixture morphology assumption is essential in a process of BC concentration retrieval.

Inheriting from in-situ retrieval algorithms of BC concentrations, the Effective Medium Approximations (EMA) of mixture morphology, including two internal mixing model Maxwell-Garnett (MG) and Bruggeman (BR), as well as an external mixing model are considered in the satellite retrieval strategy. In fact, these models have been evaluated by different aerosol component studies. China et al. (2013) proposed a case of soot particles imaged on field-emission scanning electron microscope and pointed out that most BC particles are internally coated by other material, only a little fresh and bare soot is externally mixed in the atmosphere. The mass absorption cross section of uncoated BC is about 7.5 m^2/g (Bond and Bergstrom, 2006), which is lower than the specific absorptions (10 m^2/g) of internally mixed BC modeled by Fuller et al. (1999). For BR internal mixture morphology, each aerosol component is treated as an independent without connection to others, which is not acceptable for the simulation of core-shell aerosols (Lesins et al., 2002). On the contrary, MG effective medium can be modeled as insoluble and small inclusions embedded within an aerosol particle matrix (Bohren and Huffman, 1983), which is much closer to the core-shell situation of mixture aerosol particles due to the strong adsorption and insoluble characteristics of BC aerosols. Therefore, the MG effective medium approximation is used in this study to deduce the BC surface mass concentration associated with the mixture aerosol properties retrieved from satellite signals.

Since sulfur-containing gases are released to the atmosphere primarily by fossil fuel burning, we can expect that anthropogenic black carbon is always coated by ammonium sulfate and water vapor to follow similar trends as far as their release to the atmosphere. Referring the research of Schuster et al. (2005), three-components mixture, BC coated by soluble Ammonium Sulfate (AS) and aerosol water vapor (AW), is appropriate for solutions of satellite retrieval in our study. The MG effective medium approximations can be calculated once the dielectric functions of inclusions (BC) and host (AS) are defined (Bohren and Huffman, 1983).

$$\varepsilon_{MG}(\lambda) = \varepsilon_m(\lambda)\left[1 + \frac{3\sum f_j\left(\frac{\varepsilon_j(\lambda)-\varepsilon_m(\lambda)}{\varepsilon_j(\lambda)+2\varepsilon_m(\lambda)}\right)}{1-\sum f_j\left(\frac{\varepsilon_j(\lambda)-\varepsilon_m(\lambda)}{\varepsilon_j(\lambda)+2\varepsilon_m(\lambda)}\right)}\right] \quad (1)$$

where $\varepsilon_{MG}(\lambda)$ is the effective dielectric function of the mixture; f_j indicates the volume fraction of j^{th} component in an aerosol monomer, which is defined as the volume of a constituent divided by the volume of all constituents of the mixture; $\varepsilon_m(\lambda)$ and $\varepsilon_j(\lambda)$ represent the dielectric functions of host and constituents at wavelength λ, respectively; The refractive index of the mixture aerosols can be calculated via the following relations:

$$n(\lambda) = \sqrt{\frac{\sqrt{\varepsilon_r^2(\lambda)+\varepsilon_i^2(\lambda)}+\varepsilon_r(\lambda)}{2}} \quad (2)$$

$$k(\lambda) = \sqrt{\frac{\sqrt{\varepsilon_r^2(\lambda)+\varepsilon_i^2(\lambda)}-\varepsilon_r(\lambda)}{2}} \quad (3)$$

where $\varepsilon_r(\lambda)$ and $\varepsilon_i(\lambda)$ are real and imaginary parts of MG dielectric function; $n(\lambda)$ and $k(\lambda)$ represent for the real and imaginary parts of

aerosol refractive index. It should be clarified here that the absorption properties of mixed aerosols are only attributed to the BC particles while some absorption properties of non-BC aerosols are neglected in the EMA modeling.

2.2. General organization of the forward calculations

Although the complex refractive index of aerosol monomers can be calculated through established MG procedure once a host material and the volume fractions of inclusions are given, the inverse process that retrieving the volume fraction of the inclusions attracted more focuses from the public studies. Since AERONET automated surface network provides enough information of column-averaged refractive index as well as size distributions of aerosols (Dubovik and King, 2000; Holben et al., 1998), it would be much easier to derive column BC fractions through simple cost functions (Schuster et al., 2005) of EMA. The column-integrated black carbon concentration can be converted from the retrieved fractions and the aerosol volume distribution:

$$[BC] = f_{BC}\rho_{BC}\int \frac{dV}{d\ln r} d\ln r \tag{4}$$

where r and V represent for the particle radius and particle volume concentration respectively; f_{BC} and ρ_{BC} represent for the volume fraction and density (defined as 2.0 g/cm^3) of BC, respectively.

However, to the contrary of AERONET inversion, most satellite researches focus on the inversion of aerosol optical properties. The detailed concentration cannot be retrieved from the missing physical information. The physical properties of aerosols are assumed to be constant over a specific area in most satellite retrieval strategy and these assumptions are conducive to simplifying the inversion of aerosol optical properties (Jackson et al., 2013; Levy et al., 2013). Additionally, remote sensing from spaceborne platform is strongly affected by the presence of the atmospheric aerosols along the path from sun to land targets and finally to the signals of satellite. The radiative contribution from the surface target to the satellite signal is composed as the joint of three aspects: the radiation directly reflected by the surface target; the radiation scattered by the atmosphere aerosols; and multi interactions between atmosphere and target. Recently, Radiation Transfer Model (RTM) can simulate this process through Mie scattering model (Wiscombe, 1980), which is the basic model for most satellite-based aerosol optical property retrievals. Thus, if the concentration of BC is demanded to be retrieved from the satellite signals, the model of EMA, MIE and RTM should be integrated in our study.

The schematic diagram of integrated forward model for the simulations of satellite signals are illustrated in Fig. 1. Three independent modules are involved in modeling the radiation of the satellite sensors via exchanging a set of parameters. In the previous section, we know that the physical properties of mixed aerosols, including column-averaged aerosol refractive index, can be calculated via EMA once the fraction of each component is defined. These physical properties can be used as inputs for MIE scattering model to simulate the optical properties of aerosols (extinction coefficients, asymmetry factors and absorption coefficients). Combined with the RTM, the total radiance of top atmosphere that satellites measured can be finally determined through adequate parameters of surface and geometry.

2.3. Sensitivity studies

The updated model for simulating the atmospheric radiance has been proposed in the previous section. However, it is still unclear that whether BC aerosols are sensitive in the radiative transfer process. Fig. 2 demonstrates the simulated optical properties of mixed aerosol monomers via MIE model for the wavelength of 0.675 μm under different BC volume fractions (1%–5%, 1% increments) and constant AS volume fraction (45%). It should be noted that the MIE code of single particles used in this section is inherited from the theory proposed by

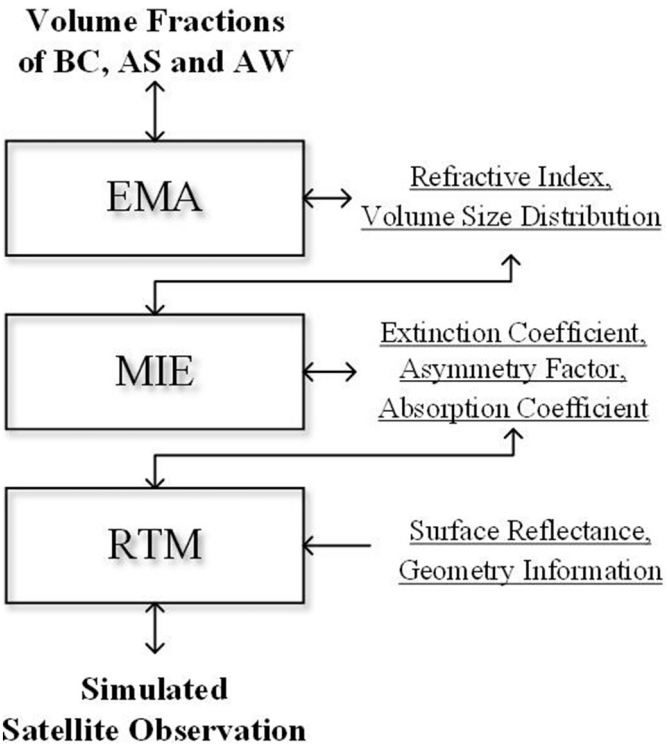

Fig. 1. Schematic diagram of the forward model for calculating the satellite-measured atmospheric radiance.

Bohren and Huffman (1983) and the initial refractive indexes of BC and AS used in EMA are summarized in Table 1. Since the vertical volume fraction of black carbon aerosols are usually proposed $< 5\%$ in other remote sensing studies (Schuster et al., 2005; Xie et al., 2017), we assume that the BC fractions do not exceed 5% in our study. Moreover, the absorption efficiency is hardly affected by non-absorbed AS aerosols (Xie et al., 2017), which means that the flexible volume fractions of AS do not further influence the final retrieved BC fractions in our study. Thus, The AS fraction was set as an average value (45%) in the sensitivity studies.

It is obvious that the simulated absorption and scattering properties of mixture aerosol monomer are different with the increasing BC volume fractions. The efficiency factor of extinction shows different levels of fluctuates as the particle radius increases. Moreover, due to the strong absorption of BC aerosols, the scattering efficiency of the mixed aerosol decreases with the climbing BC volume fractions. The absorption efficiency and asymmetry, on the contrary, increase with the increasing BC volume fractions and show obvious differences in the range of fine monomers (radius between 1 μm and 5 μm). Therefore, these discrepancies prove that the volume fraction of BC has strong sensitivity to the optical properties of mixture aerosol particles. In other words, BC fractions can be retrieved uniquely once the monomers' optical properties are defined.

Fig. 3 illustrates the simulated phase function of mixed aerosols for the wavelength of 0.44 μm (b), 0.67 μm (c) and 0.86 μm (d) for different BC fractions (1%–5%, 1% increments) and constant AS fraction (45%) via MIE model. The multi-modal log-normal size distributions of strong absorption sphere aerosols proposed by Chen et al. (2013) and same initial refractive indexes of components in Table 1 were used in these computations. It is clear that the increasing volume fraction of black carbon aerosol significantly weakens the extinction properties of mixed aerosols. Interestingly, the phase functions show a significant backward discrepancy at around $\theta > 120^\circ$ and a peak as a rise of intensity at $\theta > 160^\circ$.

Fig. 4 illustrates the influence on apparent reflectance under

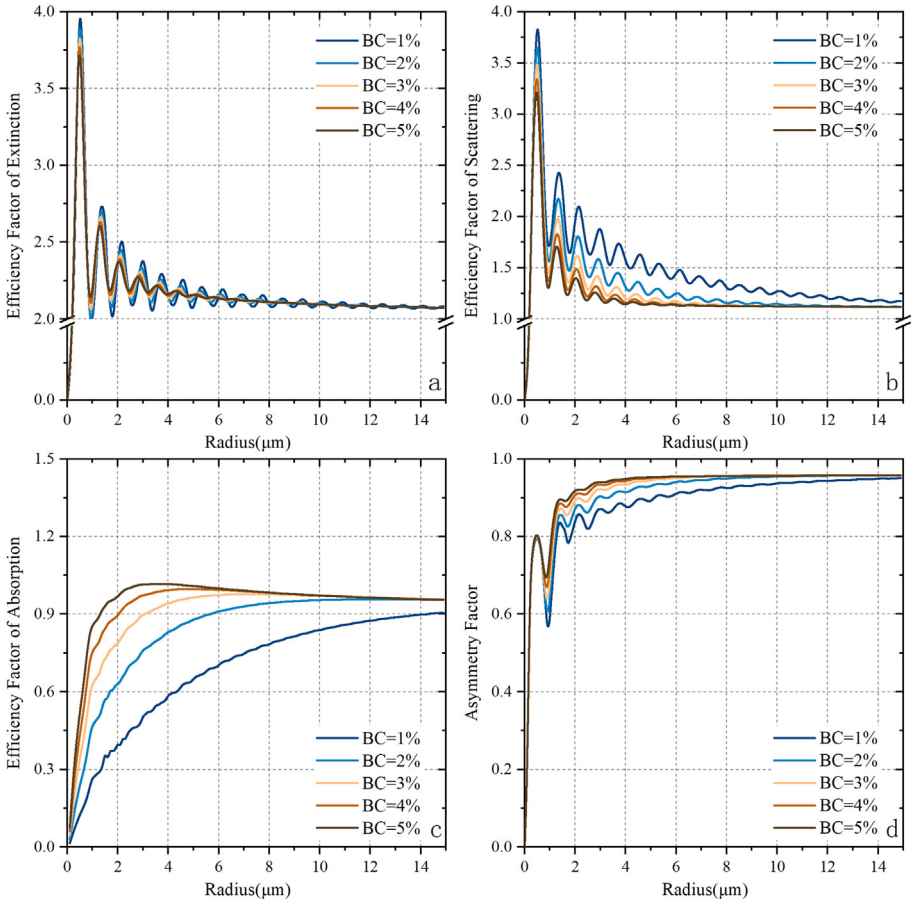

Fig. 2. Simulated optical properties of mixed aerosol monomers for the wavelength of 0.675 μm under different BC volume fractions (1%–5%, 1% increments) and constant AS volume fraction (45%) via MIE model of single particles. Including (a) Efficiency factor of extinction. (b) Efficiency factor of scattering. (c) Efficiency Factor of absorption. (d) Asymmetry factor.

Table 1
Refractive Indexes (RI) of BC and AS at four wavelengths used in this study.

	RI (440 nm)	RI (675 nm)	RI (870 nm)	RI (1020 nm)	References
BC	1.850–0.71i	1.850–0.71i	1.850–0.71i	1.850–0.71i	van Beelen et al. (2014) and Koven and Fung (2006)
AS	$1.535–10^{-7}$i	$1.525–10^{-7}$i	$1.520–10^{-7}$i	$1.530–10^{-7}$i	van Beelen et al. (2014) and Dey et al. (2006)

different aerosol optical depth (AOD) conditions exactly via the simulation of forward model. In this section, the Vector Second Simulation of the Satellite Signal in the Solar Spectrum (6SV) model is used to simulated the Top of Atmosphere (TOA) reflectance in radiative transfer process (Vermote et al., 1997). This RTM is widely applied to the inversion of aerosol optical properties on several satellites missions (Ackerman et al., 2000; Kotchenova and Vermote, 2007). Moreover, non-Lambertian surface is assumed in our simulation and thus the target Bidirectional Reflectance Distribution Function (BRDF) should be considered according to the scheme of RTM model. At present, the RossThick-LiSparseR (ROSS-LI) BRDF model is commonly used and has good universality in land remote sensing studies, which can simulate most bidirectional surface targets with considerable reflectivity correlation coefficient (0.934) and mean square error (0.016) (Li and Strahler, 1992; Schaaf et al., 2002). Hence the ROSS-LI is applied in the 6SV RTM model and the initial isotropic, volumetric and geometric-optical kernels are inherited from the studies proposed by Jiao et al. (2014).

Interestingly, many aerosol optical retrieval studies proposed that the scattering properties of aerosols are highly sensitive on dark targets (Kaufman et al., 1997), on the contrary, different volume fractions of absorptive BC aerosols are more sensitive over bright targets, which show significant discrepancies on apparent reflectance of top of atmosphere. In addition, the sensitivities of aerosols on atmospheric apparent radiation have an enhanced-weaken change compared to the one-to-one lines in these figures. Under the condition of high concentration aerosols (AOD $>$ 1.0), the intersection of the two lines are stable at about 0.100 when BC fraction is 5% and about 0.225 when BC fraction is 1%. Moreover, the comparative analyses of different AOD show that the sensitivity of BC volume fractions to satellite radiation is significantly improved under aerosol loadings. In other words, it is difficult to distinguish the satellite signal under different BC fractions in clear atmosphere (AOD $<$ 0.5). Conversely, under contaminated conditions (AOD $>$ 0.5), the discrepancies of apparent reflectance are significantly enhanced and BC fractions can be easily recognized from satellite signals. Therefore, although it is difficult to use the EMA-MIE-RTM model for performing the BC volume fraction inversion especially over the dark surface under clear atmosphere, this forward model is much suitable for the BC concentration monitoring over bright surface or polluted conditions, which has strong applicability in many polluted areas of the world (e.g. Indian Ganges plain and Eastern plains of China).

2.4. Detailed numerical inversion of algorithm

Numerical inversion of aerosol optical properties in most existing satellite retrieval algorithms have restrictions that they rely on the pre-assumed potential solutions. Indeed, these strategies can effectively

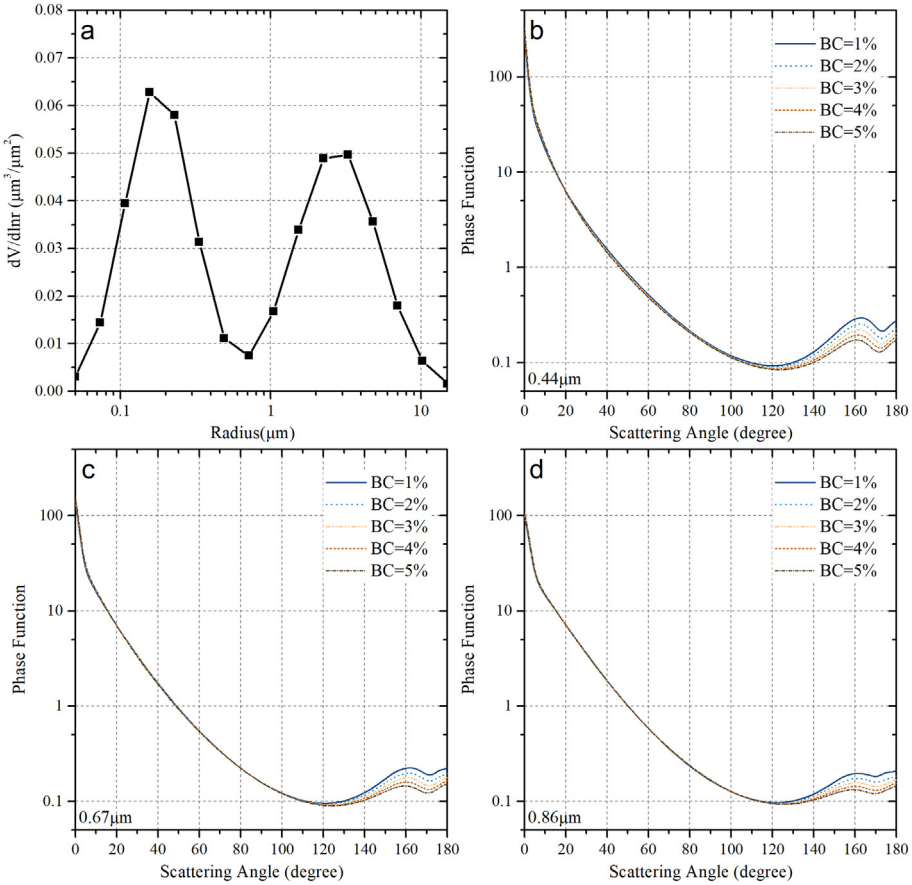

Fig. 3. Assumed size distribution of aerosols (a) (Chen et al., 2013) and simulated phase function of mixture aerosols for the wavelength of 0.44 μm (b), 0.67 μm (c) and 0.86 μm (d) for different BC fractions (1%–5%, 1% increments) and constant AS fraction (45%) via MIE model.

interpolate desired results by establishing LookUp Tables (LUTs) when the number of retrieved parameters is limited. In fact, it can be known from the Eq. (4) that since BC volume fractions and size distribution are expected to be retrieved via integrated model in our study, huge calculation of LUT establishing and inversion would be processed if the existing LUT strategy is used. Therefore, a statistically based method is needed to invert the aerosol information as commented above.

Actually, the strategy of statistically optimized algorithm was widely pursued in the earlier studies of aerosol inversion (Chowdhary et al., 2002; Martonchik et al., 1998). Dubovik and King (2000) proposed a state-of-art flexible aerosol inversion algorithm, which is widely used in worldwide AERONET in-situ sun photometer missions. Recently, this optimized statistically method has been extended to the multi-angle satellite retrieval algorithms by Dubovik et al. (2011). In contrast to the existing algorithms, this multivariable least square method (LSM) does not rely on the pre-assumed assumptions (aerosol size distribution, refractive index, optical depth etc.) and provides more complete inversion results of aerosol optical properties, which provides a suitable strategy in our study.

The detailed inversion algorithm can be found in the studies of Dubovik et al. (2011). The LSM retrieval algorithm implemented by the solution of optimum fitting of satellite observations and a priori constraints:

$$\begin{cases} f^* = f(a) + \Delta f^* \\ 0^* = S_m a + \Delta(\Delta^m a)^* \\ a^* = a + \Delta a^* \end{cases} \tag{5}$$

The first equation in (5) illustrates the relationship between the satellite measured radiation f^* and modeled radiation $f(a)$ simulated by forward model. The symbol Δf^* denotes the uncertainty in the real measurements. The expression $f(a)$ can be simply expressed as the sum of the three parts, light reflected as a result of single interaction of incident solar light with the atmosphere and surface as well as the multi scattering in the atmosphere (details are given in Lenoble et al. (2007)); The vector of unknowns a is simplified as follows:

$$[a] = [f_{BC}, f_{AS}, PSD_i],\ (i = 1\sim22) \tag{6}$$

where f_{BC} and f_{AS} represent the volume fractions of BC and AS, respectively. PSD_i denotes values of volume size distribution under 22 radii (the same as AERONET). In fact, the modeled $f(a)$ can be expanded in Taylor series:

$$f(a) = f(\hat{a}) + K(a - \hat{a}) + o(a - \hat{a})^2 \tag{7}$$

where K is the first derivative of the Jacobian matrix of the radiation transfer expression ($f(a)$). $\hat{a}$ is the close neighborhood of solution a. Additionally, satellite observations usually provide random errors in estimating the minimum inversion error. Therefore, the error term Δf^* can be expressed as follows:

$$\Delta f^* = \Delta f^*_{sys} + \Delta f^*_{ran} \tag{8}$$

where $\Delta f_{sys}{}^*$ in (9) is systematic error, a fixed value that repeats in different observations. $\Delta f_{ran}{}^*$ represents for the distribution of random noise, usually simulated by gaussian distribution as follows:

$$\begin{aligned} P(\Delta f^*) &= \prod_{i=1}^{k} P(f_i(a) \mid f_i^*) \\ &= \prod_{i=1}^{k} \left\{ [(2\pi)^m det(C_i)]^{-\frac{1}{2}} exp\left[-\tfrac{1}{2}(f_i(a) - f_i^*)^T C_i^{-1}(f_i(a) - f_i^*) \right] \right\} \end{aligned} \tag{9}$$

where C_i is the covariance matrix of i^{th} observations, det(C) is the rank of matrix C, and m is the dimension of f^*. It should be noted that the larger maximum likelihood function $P(\Delta f^*)$, the more accurate

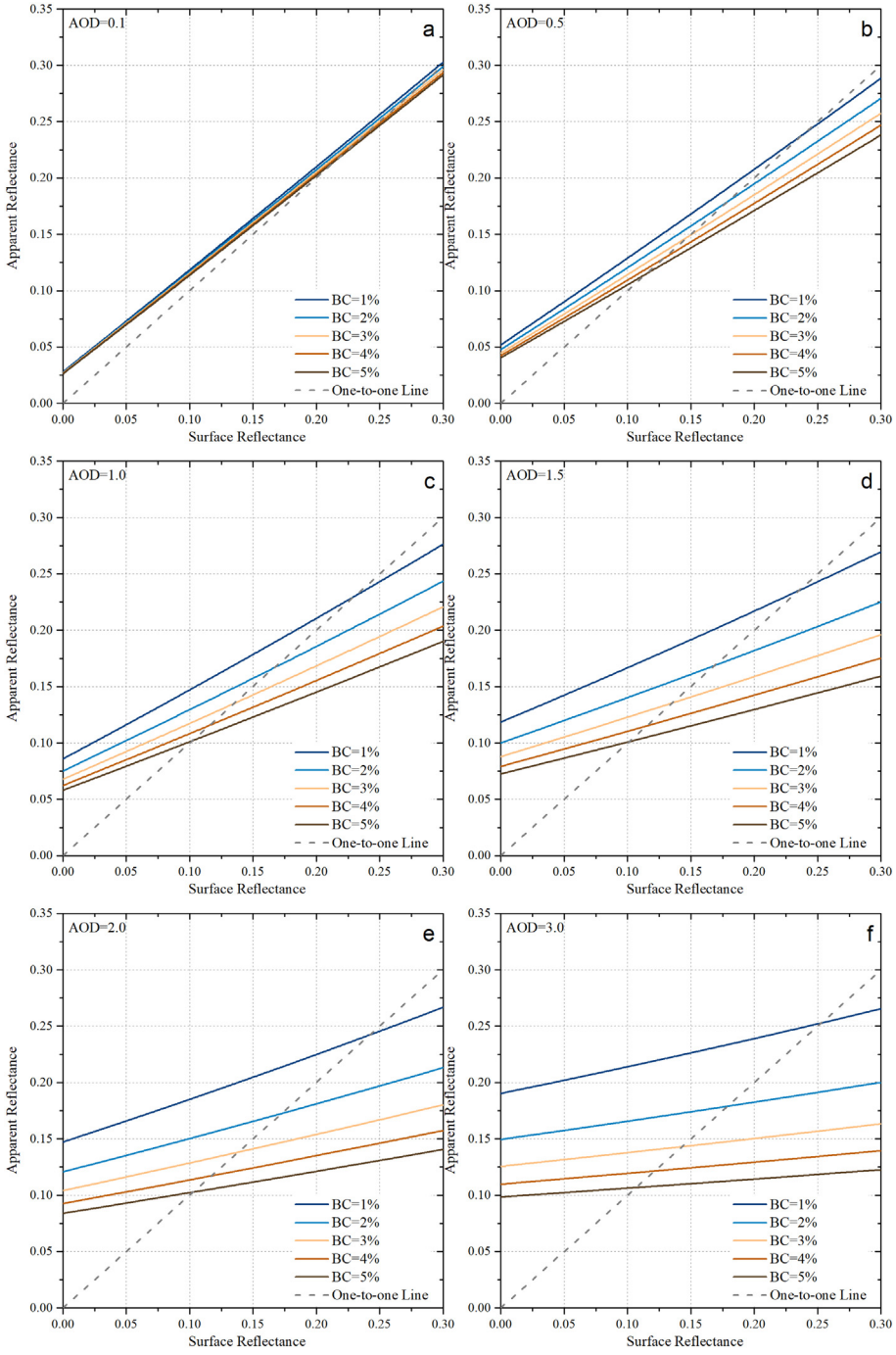

Fig. 4. Two-dimensional correlation between surface reflectance and apparent reflectance of satellite observation for the wavelength of 0.675 μm for different BC fractions (1%–5%, 1% increments) and constant AS fraction (45%) under different AOD (0.1, 0.5, 1.0, 1.5, 2.0, 3.0) (a-f). The solar zenith angle, satellite viewing angle and azimuth angle in simulation is 30°, 50° and 60° respectively. The surface reflectance, which arrange from 0.0 to 0.30, is calculated by ROSS-LI BRDF model. The grey dash line is the one-to-one line of surface reflectance and apparent reflectance.

unknown parameters we get. Therefore, the optimal solution can be expressed as:

$$2\Psi(\mathrm{a}) = \sum_{i=1}^{k} (f_i(a) - f_i^*)^T C_i^{-1} (f_i(a) - f_i^*) = min \tag{10}$$

In order to clearly assess the relative error contribution between different sensor observations, Dubovik et al. (2011) also fix the Eq. (10) by using the Lagrange multipliers γ:

$$2\Psi(\mathrm{a}) = 2\sum_{i=1}^{k} \gamma_i \Psi_i(\mathrm{a}) = \sum_{i=1}^{k} \gamma_i (f_i(a) - f_i^*)^T W_i^{-1} (f_i(a) - f_i^*) = min \tag{11}$$

where in turns,

$$\begin{cases} W_i = \dfrac{1}{\varepsilon_i^2} C_i \\ \gamma_i = \dfrac{\varepsilon_1^2}{\varepsilon_i^2} \end{cases} \tag{12}$$

where ε_i^2 first diagonal elements of the corresponding covariance

matrices C.

Noted that since the atmospheric and surface features restrict the sensitivity of each parameter in different observed geometries, it is necessary to specify the constraint equations to overcome the instability problem of the inversion algorithm (Dubovik, 2004). The second part in Eq. (5) represents the a priori smoothness assumptions used to constrain variability of retrieved characteristics. The matrix S_m in equation includes the coefficients for calculating differences of parameters under m^{th} order of finite differences; 0^* and $\Delta(\Delta^m a)^*$ represent for the vector of zeros and the vector of the uncertainties characterizing the deviations of the differences from the zeros respectively. The types of the finite differences and the correspondent values of Lagrange multipliers of size distribution and BRDF used in our algorithm for applying inter-pixel smoothness constrains follows the study of Dubovik et al. (2011), which have been clarified the definition of the matrices of multi-pixel smoothness constraints S_m and Lagrange multipliers γ_m of each retrieved parameter. And these two parameters of BC volume fraction are also inhered from the mixture refractive index due to the strong relationship between them.

The vector a^* and Δa^* included in last Eq. (5) is the vector of the uncertainties in priori estimates, which shows a possibility of using priori constraints on actual values of any retrieved parameter (Torres et al., 2017). Since these three equations in Eq. (5) can be seen as independent observation, the final cost function can be expressed as follows:

$$\begin{aligned}\Psi(a) &= \Psi_f(a) + \Psi_m(a) + \Psi_a(a)\\ &= \gamma_f \Delta f^{*T} W_f^{-1} \Delta f^* + \gamma_m (S_m a)^T W_m^{-1} (S_m a) + \gamma_a (a - a^*)^T W_a^{-1} (a - a^*)\end{aligned} \tag{13}$$

where,

$$\begin{cases} W_f = \dfrac{1}{\varepsilon_f^2} C_f; \quad \gamma_f = 1 \\ W_m = 1; \gamma_m = \varepsilon_f^2/\varepsilon_m^2 \\ W_a = \dfrac{1}{\varepsilon_a^2} C_a; \gamma_a = \varepsilon_f^2/\varepsilon_a^2 \end{cases} \tag{14}$$

In generally, the minimum of Eq. (13) can be calculated via Gauss-Newton iterative procedure:

$$a^{p+1} = a^p - t_p \Delta a^p \tag{15}$$

where Δa^p is a solution of the p^{th} so-called and can be calculated from the Levenberg-Marquardt method (Ortega and Rheinboldt, 1970):

$$\begin{aligned}\Delta a^p = &(K_p{}^T W_f^{-1} K_p + \gamma_m S_m{}^T S_m + \gamma_a W_a^{-1})^{-1} \times \\ &[K_p{}^T W_f^{-1} \Delta f^{*p} + \gamma_m S_m{}^T S_m a^p + \gamma_a W_a^{-1} (a^p - a^*)]\end{aligned} \tag{16}$$

The value of the total residual Ψ(a) should be rather small and the inversion results between different steps are more convergent (Eq. (17)) until the right solution has been found.

$$(\Psi^p - \Psi^{p+1})/\Psi^p < \varepsilon \tag{17}$$

2.5. BC surface concentration retrieval process of PARASOL observation

For the purpose of validating the proposed algorithm, Polarization and Anisotropy of Reflectance for Atmospheric Sciences Coupled with Observations from a LiDAR (PARASOL), which provides up to 16 viewing directions and radiance observations, is selected in our study. These observations can provide stable inversion results of optical properties when using the optimization algorithm (Dubovik et al., 2011; Torres et al., 2017). It should be clarified that the cloud pixels here are filtered out by using the threshold value proposed by Breon and Colzy (1999), but much more accommodating so that the heavy aerosols pollution can be detected in the image.

Actually, since the satellite observes the signals of aerosols in entire atmosphere between the ground-to-atmosphere boundary layer, it is necessary to convert column concentrations to the surface. Normally, BC column concentration (C_{column}) can be obtained by integrating the concentrations of each layer:

$$C_{column} = \int_o^H C_i(h)dh \tag{18}$$

The column BC concentration of entire ground-satellite atmospheric layer is obtained by integrating the mass of each layer. Where H represents the thickness of the whole atmospheric layer and $C_i(h)$ represents the BC mass concentration at the height of h (ranging from 0 to H) on layer i. Since the column concentration of the entire layer can be disassembled into the sum of the column concentration of different vertical layers, the surface concentration can be estimated via a simple transformation:

$$C_{surf} = C(0)\Big/h(0) \approx C_{column} * f_s/h(0) \tag{19}$$

where C_{surf} and $C(0)$ represent for the BC concentration on surface and column concentration of surface layer respectively; f_s represents the ratio of BC column concentration in the near ground layer to the whole atmospheric layer and $h(0)$ represents the height of surface layer.

Indeed, it seems unlikely to calculate the surface BC concentration based on column-integrated concentration without making assumptions of the BC vertical distribution density profiles. However, Ran et al. (2016) pointed out that BC vertical profiles displayed a vertical distribution typically shaped by a well-mixed mixing layer. BC was almost uniformly distributed within PBL typically in the daytime. Moreover, most ground-based remote sensing inversion algorithms assumed a uniform vertical profile for BC that aerosol particles mix well under the Planetary Boundary Layer (PBL) and aerosols above the PBL can be neglected due to the poor signal in satellite sensors (Dey et al., 2006; Wang et al., 2013). This means that the parameter $f_s/h(0)$ is equivalent to 1/PBLH in this case. The height of PBL (PBLH) can be globally obtained from the NCEP/NCAR Reanalysis datasets.

The general strategy of the surface BC concentration retrieval algorithm by using PARASOL observations is showed in Fig. 5. MG effective medium approximation (detailed in Section 2.1) is used for EMA and the computations of radiation fields are based on the successive order of scattering method integrated with ROSS-LI BRDF surface model (Lenoble et al., 2007). Moreover, same initial guess (a_0) was used for the unknown parameters in every pixel of PARASOL image, which described in Table 2. Additionally, it should be pointed out that six BC volume fraction results would calculated for each channel (0.44, 0.49, 0.565, 0.675, 0.87 and 1.02 μm) after the entire retrieval process, only the results on 870 nm would be chosen because the absorption of other components at this wavelength are small enough to be neglected (Sun et al., 2007; Xie et al., 2017).

3. Results and validations

3.1. Case studies of satellite retrieved BC under different sources

According to the sensitivity analyses, the algorithm proposed in this study has strong applicability in polluted conditions. Therefore, based on the PARASOL retrieval process, cases in three different sources, including agricultural activities, industrial pollution and dust-like aerosols, are tested and shown in the Figs. 6–8. The red points in these figures represent the ground fire and thermal anomalies that obtained from the Moderate Resolution Imaging Spectroradiometer (MODIS) AQUA dataset (MYD14). The in situ aerosol optical parameters are also summarized from the nearest AERONET site (Table 3).

Fig. 6 illustrates a case of agricultural activities (straw burning) over Ganges plain. According to the aerosol optical parameters obtained

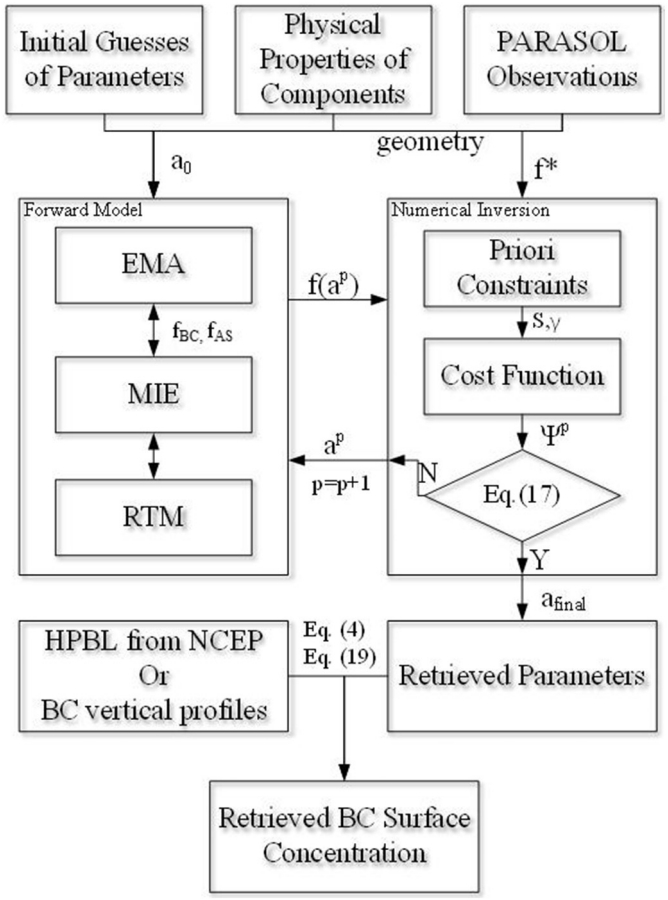

Fig. 5. The general structure of the Surface BC concentration retrieval algorithm by using PARASOL observations. The meaning of each symbols can be found in the algorithm description of Section 2.

Table 2
Initial guesses for the unknown parameters.

Aerosol parameters		Surface parameters	
$dV(r_i)/dlnr_i$	0.1	$BRDF_{iso}$	0.05
f_{BC}	1%	$BRDF_{vol}$	0.025
f_{AS}	50%	$BRDF_{geo}$	0.01

from the nearest AERONET site (Kanpur), it is clear that the atmospheric particles over the site were dominated by the strong absorptive fine particles with lower Single Scattering Albedo (SSA = 0.68) as well as higher Angstrom Exponent (AE = 0.74) and Absorption AOD (AAOD = 0.11). Referred to dense fire anomalies appeared in upwind areas, it can be concluded that the pollution in this area is dominantly produced by biomass burning activities. From satellite retrieval, higher BC concentration can be retrieved along with the shape of the smoke, and the spatial distribution shows a tendency of spread around.

In contrast, air pollution in eastern China is dominated by complicated aerosol types and sources (Li et al., 2017), the pattern of BC in this area is consistent with the industrial emissions (Fig. 7). Base on the aerosol parameters obtained from the nearest AERONET site (Beijing-RADI), since more non-absorbent components are mixed with BC, a weaker absorption aerosol (SSA = 0.85) and minor particles (AE = 1.40) can be found over the site compared to the characteristics over Kanpur. Even though less fire anomalies can be found in this area, higher BC concentration can be retrieved from satellite along with high aerosol tendency.

As to demonstrate the applicability of proposed algorithm in aerosol identification, a natural case over Thar Desert is proposed in Fig. 8. Compared with agricultural burning and industrial activities, the atmospheric particles over desert AERONET site (Jaipur) were dominated by the dust-like aerosols (AE = 0.07) with higher SSA (0.98). The AAOD over the site is only 0.01 even if the AOD is extremely high in this area (0.83). Therefore, lower regional BC concentration is shown in the BC retrieved image and the spatial variability of results over the region is relatively small.

3.2. Comparison with in situ BC observation

In order to study the accuracy of the proposed retrieval algorithm, in-situ surface mass concentration of BC should be selected in the validation study. Xu et al. (2018) collected 32 monthly averaged measurements of BC concentrations from other studies over South Asia, which demonstrate a wide range of surface backgrounds, such urban, rural, coastal and high altitude (Fig. 9). In addition, the Monthly BC concentration simulated by the Modern-Era Retrospective Analysis for Research and Applications, Version 2 (MERRA-2) is also used for validation. This model is intended as an intermediate reanalysis, one that not only leverages recent developments in modeling and data assimilation but also provides a longer-term goal of developing an integrated Earth system analysis capability that couples assimilation systems for the atmosphere, ocean, land, and chemistry. Additionally, in order to be consistent with the spatial resolution of MERRA-2, the spatial resolution of PARASOL retrievals (6 km) should be resized to 66 km (10 * 10 px) in this study.

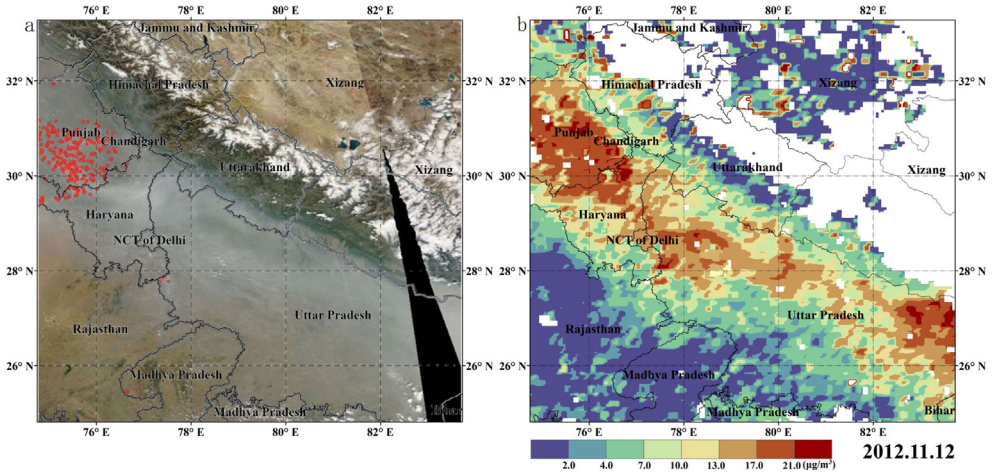

Fig. 6. Case studies of agricultural activities over Ganges plain (Nov. 12th, 2012) based on the PARASOL BC retrieval (b). RGB images (a) and the fire and thermal anomalies (red points) are obtained from the MODIS AQUA dataset (MYD021km and MYD14, respectively). (For interpretation of the references to colour in this figure legend, the reader is referred to the web version of this article.)

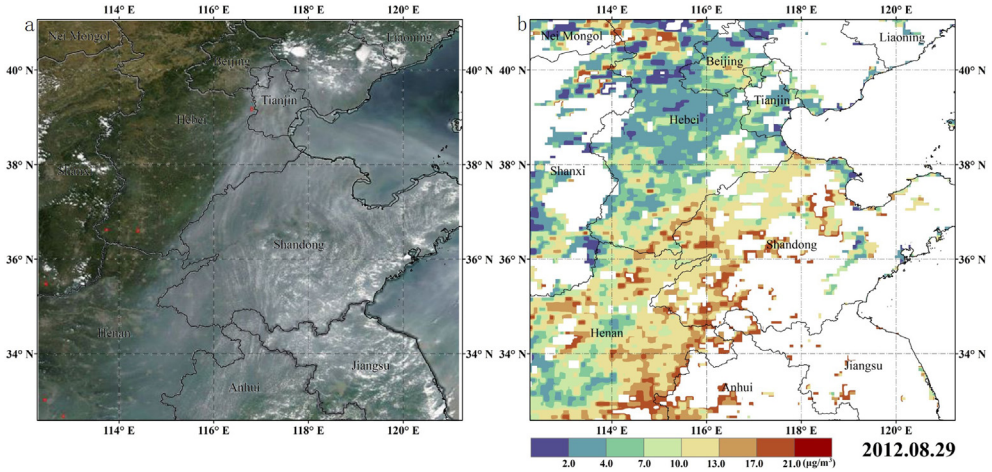

Fig. 7. Case studies of industrial pollution over East China (Aug. 29th, 2012) based on the PARASOL BC retrieval (b). RGB images (a) and the fire and thermal anomalies (red points) are obtained from the MODIS AQUA dataset (MYD021km and MYD14, respectively). (For interpretation of the references to colour in this figure legend, the reader is referred to the web version of this article.)

Fig. 10 illustrates the comparisons of monthly BC surface mass concentration of 2012 over these sites. It is clear that the results retrieved by satellite and simulated by MERRA-2 share a similar general correlation (R) and Root Mean Squared Error (RMSE), which illustrating the reliability of estimated BC in this study. Moreover, for the coverage of the results, the concentration of BC simulated by model can cover the entire region (Accounts = 100%), while only 86.1% covered for the satellite retrievals due to the cloud contamination in the remote sensing image. Interestingly, it is shown that these two products demonstrate different levels of accuracy under different levels of BC mass concentration. The slope of the linear fitting calculated by retrieved BC is 0.78 while the one fitted by MERRA-2 is only 0.28. It means that the satellite inversion has higher accuracy under extreme biomass burning activities. The surface mass modeled by MERRA-2 is significantly underestimated since the emission inventories and optical properties in polluted atmospheric environment are not generating enough BC absorption in the model (Koch et al., 2009). However, the lower BC surface concentration calculated by satellite retrieval has greater deviation compared with MERRA-2 simulation (the intercept is 3.85 and 1.11 respectively), which indicates that the satellite inversion significantly exaggerates the results especially in the case of clear conditions. These overestimations lead a greater average bias of retrieved BC compared to MERRA-2's.

In fact, the accuracy characteristics of these two products are also reflected in different seasons. Fig. 11 illustrates the validation of monthly BC surface concentration between satellite retrieved and ground observed over South Asia on dry (Oct.–May) and rainy season (Jun.–Sep.) respectively. In the season with frequent biomass burning activities over Ganges plain (dry season), the concentration of PARASOL retrievals shows a higher correlation coefficient (R = 0.75), linear slope (0.71) and RMSE (4.04) compared with MERRA-2 products. However, in rainy season, the inferiority of satellite inversion on coverage and accuracy are magnified due to the extreme clear and wet weather over the region. Therefore, it can be concluded that the results of satellite retrieval can effectively detect the concentration of BC under biomass burning activities, which is better than the MERRA-2 model simulation.

Table 3
Aerosol optical characterization data of nearest AERONET sites in three case studies.

Aerosol parameters	Nov. 12th, 2012	Aug. 29th, 2012	Jun. 26th, 2012)
Site	Kanpur	Beijing-RADI	Jaipur
AOD (870nm)	0.34	0.12	0.83
AE (870/440)	0.74	1.40	0.07
SSA (870 nm)	0.68	0.85	0.98
AAOD (870 nm)	0.11	0.02	0.01

Additionally, satellite observations are also significantly affected by surface reflectance, the sensitivity of BC concentration on radiative signals is different under different types of surface. Table 4 summarized the parameters of validation between satellite retrievals and in situ observed under different surface backgrounds. The coverage of satellite inversion in the plain area is better than the Plateau and the Himalayas (Account = 67%) in South Asia, with > 80% coverage in urban, rural and coastal region. Moreover, BC retrievals have acceptable correlation

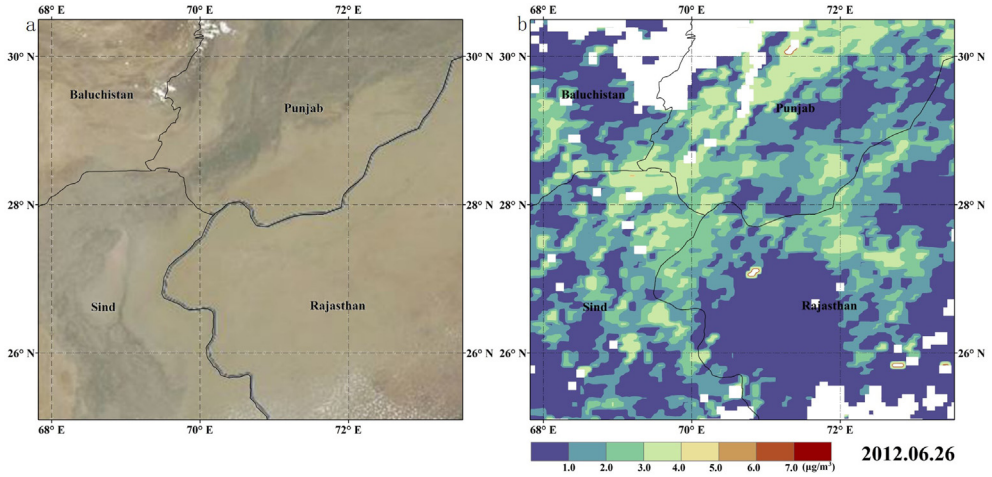

Fig. 8. Case studies of dust-like aerosols over Thar Desert (Jun. 26th, 2012) based on the PARASOL BC retrieval (b). RGB images (a) and the fire and thermal anomalies (red points) are obtained from the MODIS AQUA dataset (MYD021km and MYD14, respectively). (For interpretation of the references to colour in this figure legend, the reader is referred to the web version of this article.)

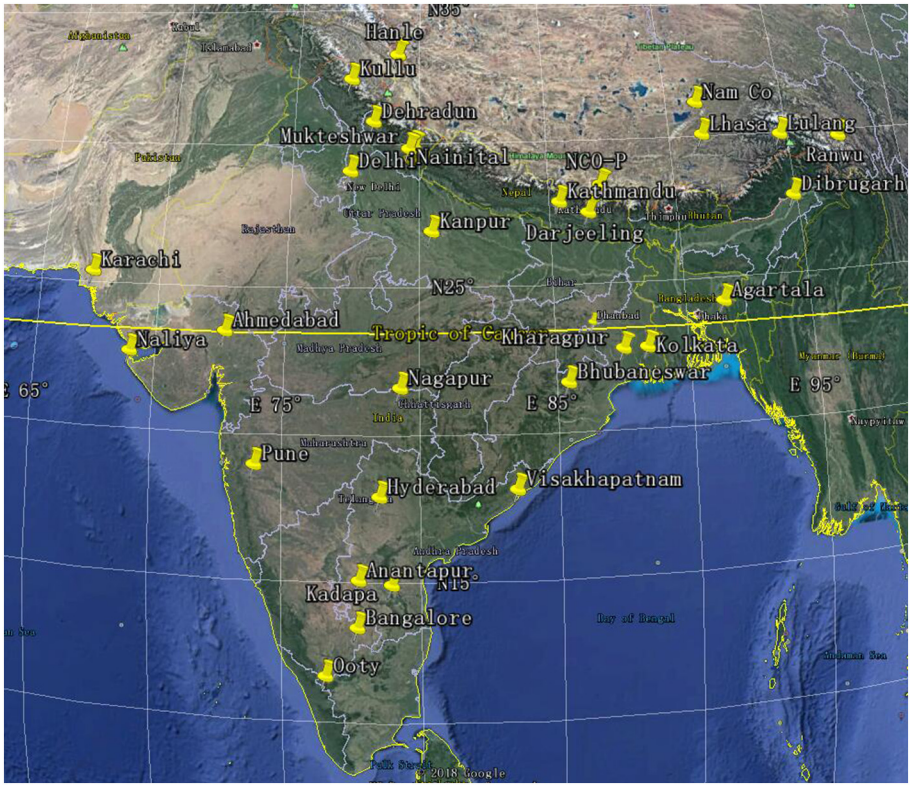

Fig. 9. The location of in-situ surface mass concentration of BC aerosols (Xu et al., 2018).

coefficient under the urban (0.70), rural (0.79) and coastal (0.69) surfaces compared to the high-altitude area (0.57). RMSE and average bias also show similar accuracy over these three surfaces. In addition, based on the merits of higher accuracy in polluted condition, the slopes of the linear fitting (k) have a considerable value in all areas. However, the retrievals are extremely unstable over coastal and high-altitude area that the confidence intervals (95%) for the slopes are large in these areas. It should be noted that even if the fitted intercepts (b) are > 3.00 in all situations, the accuracy of lower BC concentration in high aerosol forcing areas (anthropogenic aerosols in urban and sea salt aerosols in coastal) is better than that in other two clear areas.

3.3. Closure validation of BC retrieval algorithm

It can be known from the studies of cases and validation that the results of inversion using the proposed algorithm can effectively separate the contribution of BC aerosols from the pollutants. However, the inversion results are still highly uncertain especially under specific conditions compared to ground-based observations. Therefore, since the column-integrated black carbon concentration can be converted from retrieved fractions and volume distribution (Eq. (4)), a series of closure validation tests for these two parameters should be performed to verify the performance of the designed approach and to provide conclusive illustration of error sources.

Fig. 12 (a) illustrates the correlation between modeled and assumed BC fractions under four aerosol loadings (from 0.1 to 2.0), respectively. Here, “modeled” denote the results retrieved from forward modeled satellite signals based on in situ observation. AOD is considered as an independent tunable variable, BC is always assumed to be coated by 45% AS and the values chosen for the size distribution and surface

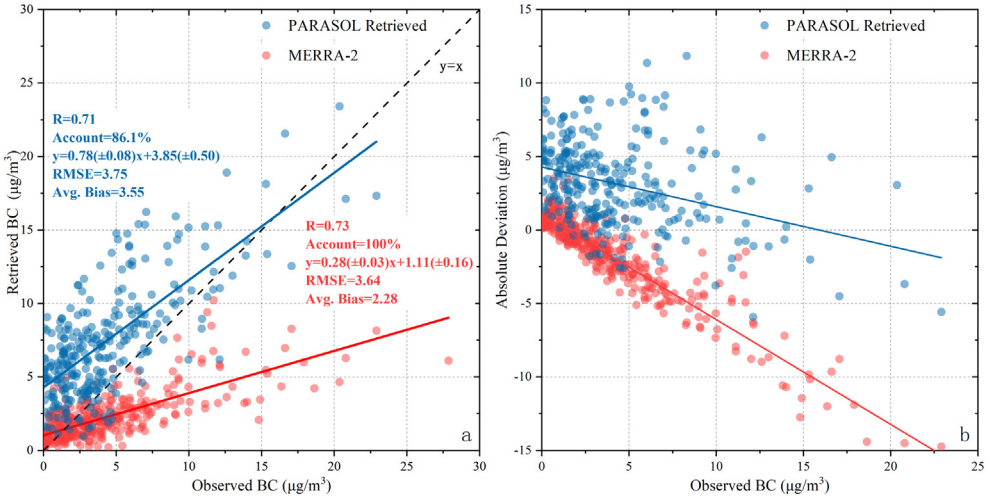

Fig. 10. Comparison of monthly BC surface mass concentration between satellite retrieved and ground observed over South Asia (a) and absolute deviation from the in-situ observation (b). The red and blue points in the figure represent the results simulated by MERRA-2 model and retrieved by our algorithm, respectively. The numbers in parentheses represent 95% confidence intervals. (For interpretation of the references to colour in this figure legend, the reader is referred to the web version of this article.)

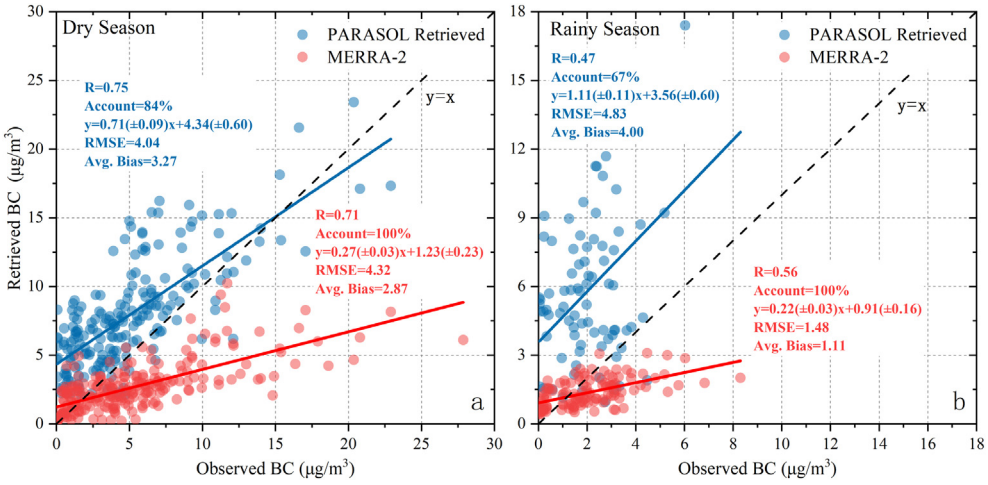

Fig. 11. Comparison of monthly BC surface mass concentration between satellite retrieved and ground observed over South Asia on season of dry (a) and rainy (b). The red and blue points in the figure represent the results simulated by MERRA-2 model and retrieved by our algorithm, respectively. The numbers in parentheses represent 95% confidence intervals. (For interpretation of the references to colour in this figure legend, the reader is referred to the web version of this article.)

Table 4
Comparison of monthly BC surface mass concentration between PARASOL retrieved and ground observed over different surface backgrounds. The numbers in parentheses represent 95% confidence intervals.

Surface background	R	Act.	k	b	RMSE	Avg. bias
Urban	0.70	85%	0.79(± 0.17)	3.21(± 1.20)	3.84	2.87
Rural	0.79	83%	0.74(± 0.15)	4.05(± 1.00)	3.91	3.14
Coastal	0.69	84%	0.90(± 0.37)	3.29(± 1.79)	3.65	3.03
high altitude	0.57	67%	0.89(± 0.48)	4.89(± 1.00)	5.08	4.64

albedo are generally close to the observations reported from the AERONET site (Beijing).

It is realized that the modeled fractions have a general correlation with simulation. The average relative uncertainties can be controlled within 10% when the aerosol loading is high (AOD = 2.0). Conversely, large uncertainties can be found under the clear sky. In fact, Xie et al. (2017) pointed out that the Imaginary part of Refractive Index (IRI) is highly relates to the absorbing aerosol components. They proved that the accuracy is considerable via EMA simulation. Therefore, these deviations of fractions can be explained by the fact that the contribution of low aerosol loadings into radiation is negligible in the satellite view and even minor perturbations of the observation may significantly affect the final retrieval results.

Apart from the fractions of BC aerosols, the volume size distribution is another important impact that influences the final calculated concentration. Fig. 12 (b) demonstrates the validation between observed and modeled volume size distribution with averaged discrepancy by using the selected AERONET data. Interestingly, compared with the observed distribution, the characterizations of fine mode aerosol are more accurate, while the characterizations of coarse mode aerosol have greater uncertainties with maximum 0.2 bias. These deviations will seriously exaggerate the results of BC concentration. Actually, Torres et al. (2017) proposed the same point that the characterizations of fine mode aerosol properties retrieved by statistically optimized inversion algorithm are accurate, with 5% uncertainties for fine mode volume size distribution while 10% for the cases with a prevailing coarse mode. Additionally, Dubovik et al. (2011) also pointed out that the retrieval of size distribution seems to be rather dependent on AOD by using the optimized inversion algorithm, which further affects the accuracy of BC concentration in clear conditions.

Additionally, surface albedo, which coupled with atmospheric aerosol signals, is another main factor that influenced the final retrievals. The uncertainties of surface albedo will lead substantial deviates for BC concentration from the true value. This optimized retrieved parameter has been fully tested under different aerosol loadings by Dubovik et al. (2011), which showed reasonable results that the retrieved surface albedo in each band is almost close to the observed value. Therefore, the uncertainty of our retrieved model is mainly dominated by the aerosol parameters.

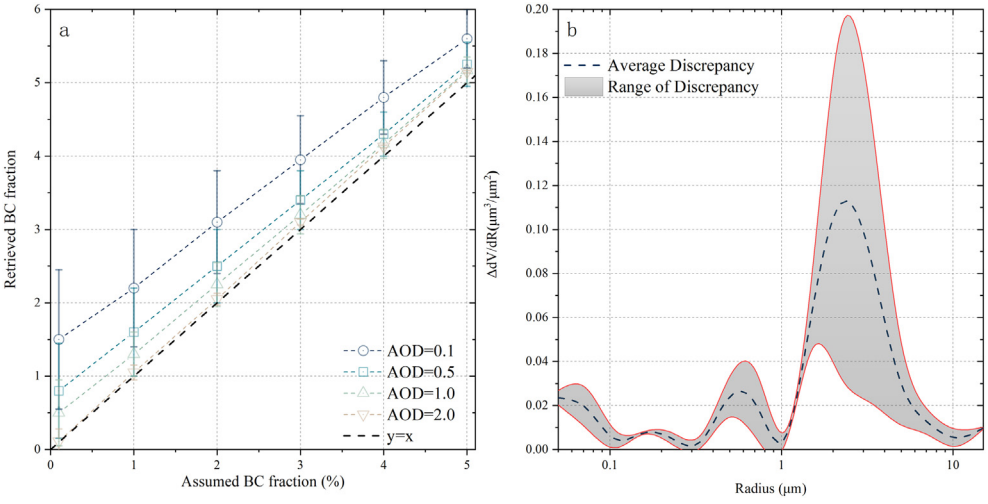

Fig. 12. Retrieval of BC fractions (0.1%, 1%, 2%, 3%, 4%, 5%) for 4 different aerosol loadings from 0.1 to 2.0 (a); Averaged discrepancy between Beijing observed and modeled volume size distribution. (b). Values chosen for the size distribution and surface albedo are generally close to the values reported from the AERONET site (Beijing) and the volume fraction of AS in each test are fixed to 45%.

4. Discussion

4.1. Uncertainties caused by uniform vertical profile for BC

The black carbon aerosol is assumed to be uniformly distributed without delimiting vertical profiles in our algorithm, as well as the concentration above the PBL is neglected due to the lower concentration in upper stratosphere (Samset and Myhre, 2011). In fact, the vertical BC aerosol concentration distribution is not uniform from the ground to space in the real status. Therefore, the uncertainties of the retrieved BC surface results are significant when defining the f_s in Eq. (19). Currently, the vertical characteristic of BC can be obtained by actual observation or simulated by Dynamics – Chemistry models. Single-point observations have certain limitations in space and are not suitable for large-area inversion of satellite remote sensing while modeled BC vertical concentrations via chemistry models coupled with dynamics models can provide more complete space coverage. Thus, in order to discuss the uncertainties of the uniform vertical profile assumption on retrieval results, monthly PBLH and BC vertical profiles simulated by Model for Ozone and Related chemical Tracers, version 4 (MOZART-4) were selected over four different backgrounds (Delhi for urban, Agartala for rural, Bhubaneswar for coastal and Mukteshwar for high altitude) in South Asia (Fig. 13).

On the one hand, it is point out that the column fractions of BC (column concentration of each level/total column concentration) below PBL in most cases are uniform, the underestimation of surface-level column concentration caused by this assumption is lower than 5%. Additionally, the vertical BC column fraction distribution in rainy season (< 1%) is more stable than that in dry season (1%–5%).

On the other hand, although the concentration of BC above PBL is much lower, neglecting the high-altitude BC will cause a huge overestimation for inversion due to the wider altitude above PBL. The neglected proportion of BC in the column concentration varies seasonally and ranges from 5% to 80%, which means that the surface BC concentration will be overestimated by 0.05–4 times compared with the modeling results. Nevertheless, since the emission inventories and optical properties for the smoke are not generating enough BC absorption in the MOZART model (Koch et al., 2009), the modeled estimation shows significant underestimation on surface BC concentration, the actual uncertainty will be much lower than this interval. Additionally, since the concentration of BC above PBL almost unchanged seasonally, decreasing in the proportion of surface BC leads to an opposite change above the PBL, which will cause a huge overestimation when this part is neglected in retrieval. Conversely, for high concentrations of surface BC, this uncertainty is less pronounced due to the compressed proportion at upper level. This conclusion also fully proves that our inversion results have higher accuracy under extreme biomass burning activities.

4.2. Uncertainties caused by neglecting light-absorbing aerosol particles

In the retrieval algorithm, the absorption property of aerosol is only attributed to the BC particles, while some light absorbed aerosols, such as brown carbon (BrC), and dust (DU), are neglected due to the weak absorption in infrared and near infrared channels, which will expand the absorption of BC in the atmosphere and overestimate the final concentration.

Fig. 14 illustrates the uncertainties of neglecting brown carbon (BrC) and dust aerosols on TOA (infrared channels). Considering the absorption of these two aerosols, the simulated TOAs will be significantly reduced especially under higher AOD and volume fractions. Without considering the absorption of these two components, TOAs overestimated by about 0.09/0.13 under the extreme aerosol forcing (AOD = 3.0) when the volume fraction of BrC/DU is 90%. These uncertainties of TOAs will result in an overestimation of BC concentration by 31%/43% in these extreme non-BC polluted conditions.

In addition, the absorption of each aerosol hardly affects the finally BC volume fractions under lower AOD and non-BC volume fractions, the uncertainties are lower than 5% under these conditions. For example, for the dust case of Fig. 8, since there are a lot of dust aerosols mixed with BC over Thar Desert, the uncertainties of the retrievals are significant in this case study. However, the AOD over the site is much lower than 3.00 (AOD = 0.83) according to the AERONET observation over Jaipur, thus it is acceptable that the uncertainties caused by light-absorbed dust in this case is approximate lower than 10%.

4.3. Uncertainties of using effective medium approximation model in retrieval

The shape of mixed aerosol monomers used in this study are assumed to be spherical in all conditions. However, results of in situ measurements and laboratory studies indicate that freshly aggregated BC particles tend to be coated with a thin layer of other aerosol component through the coagulation and condensation of secondary aerosol compounds (China et al., 2015; Wang et al., 2017). Large variations in BC optical properties have been indicated by further modeling studies due to the observed complex internally-mixed structures (He et al., 2015; Scarnato et al., 2013). Thus, using the MG EMA could lead to uncertainties when simulating the optical properties of internally mixed BC.

Referring to another research of our team (Wu et al., 2018), realistic BC particle morphologies during aging can be qualified for modeling BC optical properties depend on the fractions of BC/non-BC materials, which indicates the mixing of aggregated BC monomers with larger non-BC components in the individual particles, resulting in more compact BC structures and various mixing states. In order to know how the non-spherical structure affects the retrieval in the present study and how much uncertainty would be introduced to the retrieval by this issue, a superposition T-matrix method and code (MSTM) (Mackowski and Mishchenko, 2011) is used to calculate the optical properties of the aggregate model for the BC-containing aerosols.

Fig. 15 showed simulated optical properties (Efficiency factor of extinction and Efficiency factor of scattering) of mixed aerosol monomers for the wavelength of 0.532 μm under two different BC fractions (1% and 6.3%) via the simulation of MG-Mie and MSTM. In fact, these two physical parameters have a good consistency especially when the effective radius is smaller than 0.5. However, optical properties modeled by spherical model still have significant inconsistency when the radius is larger than 0.5. The maximum uncertainties of extinction and scattering properties are both approximately to 20% when the fraction of BC is 1.0%. In comparison, the maximum discrepancies of these parameters between MG EMA and MSTM are increased to 30% under higher BC fractions (6.3%).

In summary, the uncertainties of proposing uniform vertical profile for BC, neglecting light-absorbing aerosols and using spherical EMA models are different based on the amount of black carbon aerosol loadings. By ignoring the propagation error in forward simulation, the maximum standard deviations caused by these three uncertainties on low BC aerosol volume fractions (f_{BC} < 1%) are 0.8%, 0.35% and 0.2% while these deviations will change to 0.25%, 0.05% and 1.5% under higher BC fractions (f_{BC} > 5%), which further proved the accuracy of the algorithm in extreme biomass-burning pollution.

5. Conclusions

Black Carbon in the atmospheric environment is an important part of the anthropogenic aerosol, which has strong direct and indirect radiative impacts on climate change. Recently, most satellite remote sensing studies on aerosol detection are limited to inversion of aerosol optical properties and most aerosols components studies using remote sensing signals are only based on in situ observations. The feasibility and algorithm of component concentrations retrieved from satellite radiative signals are still uncertain. Therefore, this paper has discussed

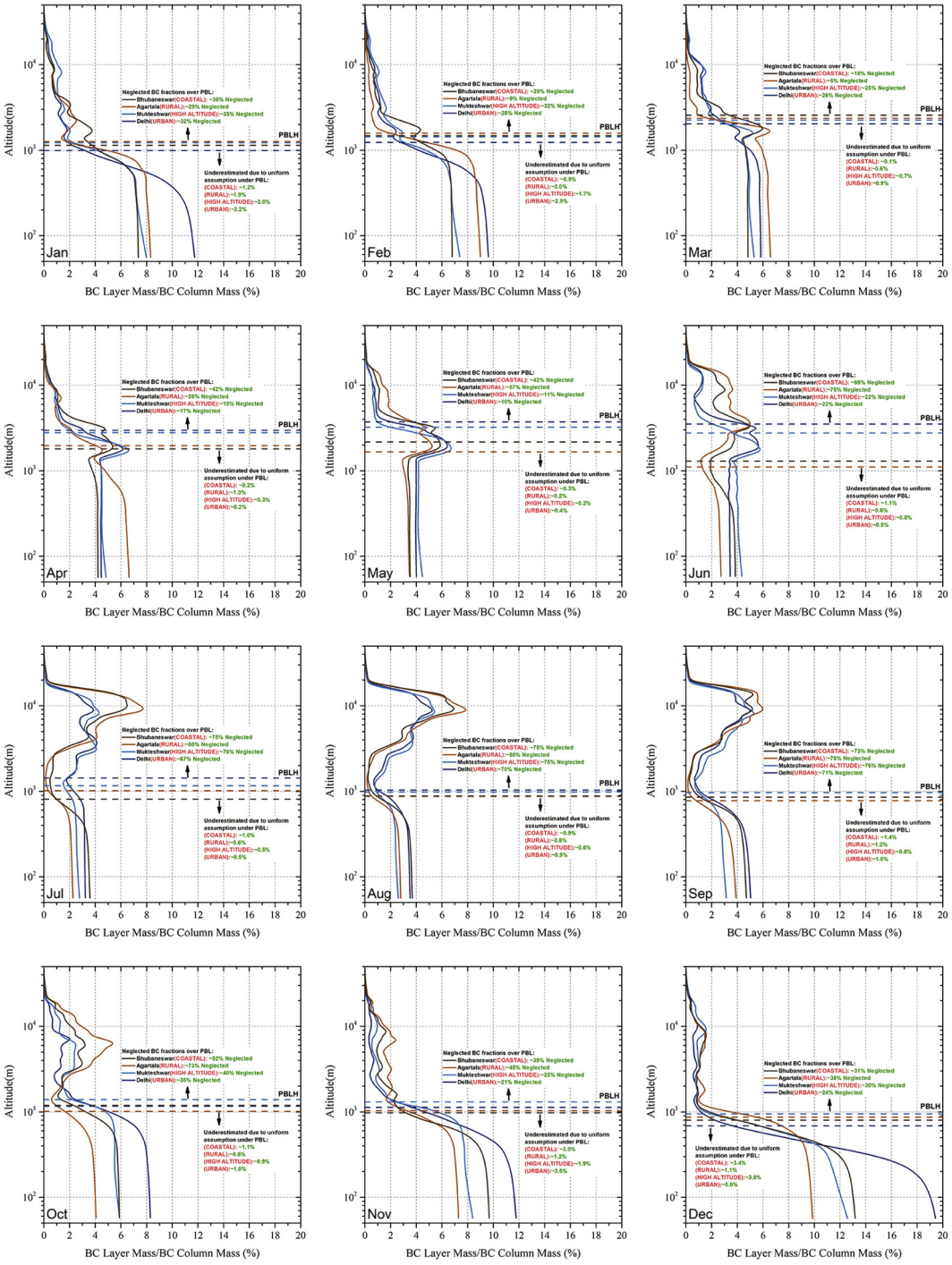

Fig. 13. Monthly MOZART-4 PBLH and BC vertical fraction profiles (column concentration of each layer/total column concentration) over four different backgrounds, including Delhi for urban, Agartala for rural, Bhubaneswar for coastal and Mukteshwar for high altitude. The uncertainties of two assumptions, uniform profile below the PBL and neglecting BC above the PBL, are also summarized in each figure.

in detail for an algorithm developed for deriving the surface concentration of BC aerosol from satellite observations without any integration of chemistry model.

In order to simulate the satellite atmospheric radiation field from BC aerosols, an optimized forward model was updated by using the integral modules of effective medium approximations, Mie and radiative transfer. The physical properties of mixture aerosols, which is used as inputs for MIE scattering model, can be calculated via EMA once the fraction of each aerosol component is defined. Combined with the Mie and RTM, the total radiance of top atmosphere that satellites measured can be finally determined through adequate information of surface reflectance and geometry.

The performance of modules in developed forward model has been demonstrated by assumed BC fractions. A series of sensitivity tests of physical and optical properties was conducted by applying the Mie and RTM modules under different levels of aerosol concentration and surface backgrounds. The results showed that the volume fraction of BC has strong sensitivity to the optical properties of mixture particles. The absorption efficiency showed an obvious difference especially in the range of fine particles and also performed a significant backward

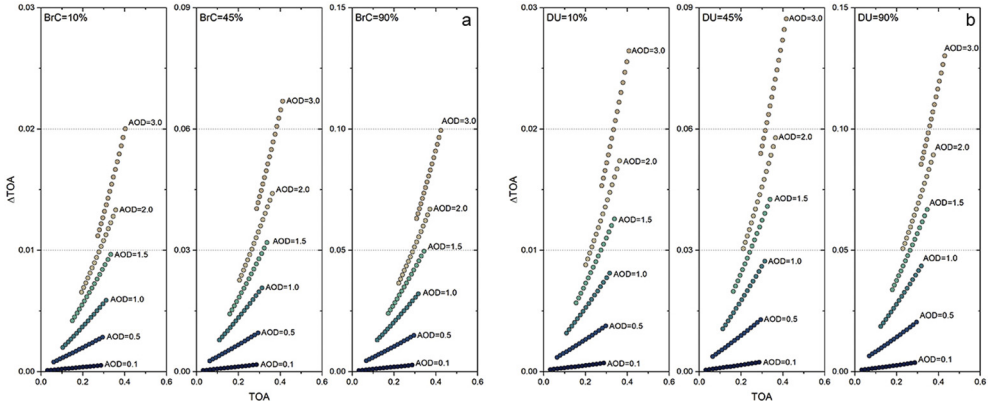

Fig. 14. The uncertainties of neglecting brown carbon (BrC) and dust aerosols on TOA (infrared channels) under different AOD (0.1, 0.5, 1.0, 1.5, 2.0, 3.0). The aerosol volume fractions for both two aerosol components were set to 10%, 45% and 90%, respectively. The X-axis represents the simulated TOA from 6SV without considering the absorption characteristics of light-absorbed aerosol. The Y-axis represents the TOA difference between considering the light-absorbed aerosol and neglecting their absorption characteristics. (For interpretation of the references to colour in this figure legend, the reader is referred to the web version of this article.)

sensitivity in specific bands. In addition, the comparative analyses of different AOD and surface reflectance showed that the sensitivity of the BC fractions to satellite radiation is significantly improved over bright targets or under polluted atmospheric conditions, which lead an embarrassment for performing BC fraction inversion especially under clear atmosphere by using the forward model.

For the interpolation calculation of forward model, a statistically optimized inversion algorithm developed by (Dubovik et al. (2011)) was used in our study. This proposed retrieval discarded precalculated look-up tables method and optimized the deviations to fit realistic observations by satellite radiative transfer process under conditions of observation. In this study, we modified the inversion forward model and retrieved parameters to directly calculate the surface concentration of BC and applied this algorithm to the multi-angle PARASOL observations. Three high aerosol loads cases including agricultural activities, industrial pollution and dust-like aerosols, were analyzed accompanied with sun photometer measurements, which showed an encouraging result that our algorithm performed a strong ability of aerosol detection under polluted atmosphere.

In addition, the consistencies of retrieved results with in situ observations were also investigated by validation and closure studies. The comparison of the derived BC concentration with available in situ observations over South Asia indicated an encouraging consistency in our study. Compared with MERRA-2 simulation, the accuracy of retrieved results demonstrates different trends under different levels of BC mass concentration, which had higher accuracy under extreme biomass burning activities while exaggerates the results in the case of clear conditions. This conclusion was further confirmed in the segmentation validation under the conditions of different seasons and surface backgrounds. Moreover, the source of the retrieval error was analyzed via closure validation by using the simulated satellite signals. The results showed quite good agreements for BC fractions, with the coefficients closed to 1.0 especially under high aerosol loadings. Additionally, the size distribution of fine mode aerosol was more accurate while the characterizations of coarse mode aerosol have greater uncertainties. These discrepancies increased as the decreasing aerosol concentration, which further exaggerated the final results of BC concentration as a whole.

Finally, since the BC surface mass retrieved algorithm in this study was proposed under an ideal atmospheric aerosol condition, the uncertainties of several assumptions, including proposing uniform vertical profile for BC, neglecting light-absorbing aerosols and using spherical EMA models are discussed in the last section. The maximum standard deviations caused by these three uncertainties on low BC aerosol volume fractions ($f_{BC} < 1\%$) are 0.8%, 0.35% and 0.2%, respectively. But these deviations will change to 0.25%, 0.05% and 1.5% under higher BC fractions ($f_{BC} > 5\%$). These discussions are conducive to error sources analyzation and algorithm improvements. In future research, more comprehensive studies for testing and tuning the developed BC retrieved algorithm are planned in future efforts. The capabilities of satellite remote sensing in aerosol monitoring would be extended by enriching the aerosol component mixture model in follow-on studies.

Acknowledgments

This research has received funding from the National Key Research

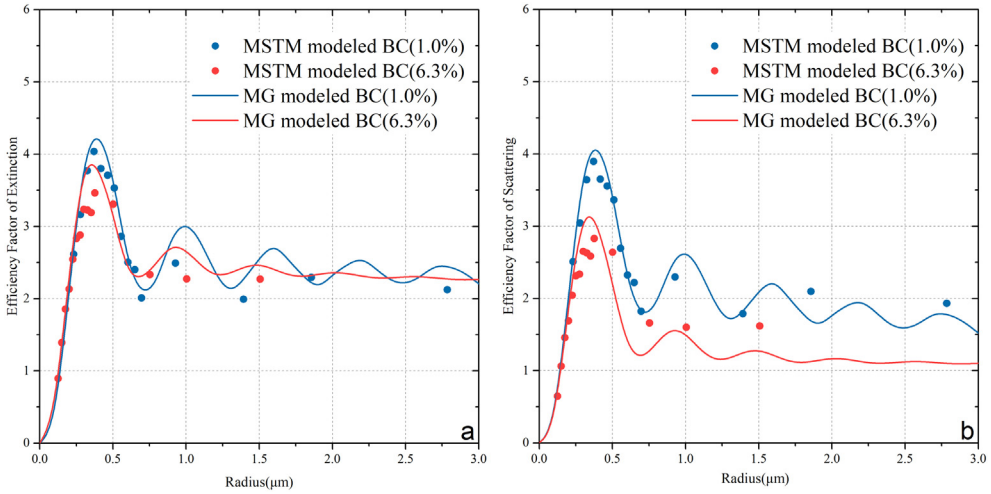

Fig. 15. Simulated optical properties of mixed aerosol monomers for the wavelength of 0.532 μm under 1% and 6.3% BC fractions via the simulation of MG-Mie and MSTM. Including (a) Efficiency factor of extinction. (b) Efficiency factor of scattering.

and Development Program of China under grant 2017YFC0212302; This research also supported by the National Natural Science Foundation of China (Grant 41575106) and Science and Technology Planning Project of Guangdong Province of China (Grant 2017A050506003). The authors would like to thank the National Aeronautics and Space Administration (NASA) and PHOTONS for providing AERONET sites data; The authors thank the ICARE Data and Services Center for providing access to the PARASOL data and products as well as NASA for providing the MODIS products and MERRA-2 reanalyzes data; We thank Dr. Daniel Mackowski and Dr. Michael Mishchenko for the code of the superposition T-Matrix method (MSTM) (http://www.eng.auburn.edu/users/dmckwski/scatcodes/). We also thank the Oleg Dubovik for providing general assistance on statistically optimized inversion code.

References

Ackerman, A.S., Toon, O.B., Stevens, D.E., Heymsfield, A.J., Ramanathan, V., Welton, E.J., 2000. Reduction of tropical cloudiness by soot. Science 288, 1042–1047.
Arola, A., Schuster, G., Myhre, G., Kazadzis, S., Dey, S., Tripathi, S.N., 2011. Inferring absorbing organic carbon content from AERONET data. Atmos. Chem. Phys. 11, 215–225.
Bohren, C.F., Huffman, D.R., 1983. Absorption and Scattering of Light by Small Particles. John Wiley and Sons, New York.
Bond, T.C., Bergstrom, R.W., 2006. Light absorption by carbonaceous particles: an investigative review. Aerosol Sci. Technol. 40, 27–67.
Bond, T.C., Charlson, R.J., Heintzenberg, J., 1998. Quantifying the emission of light-absorbing particles: measurements tailored to climate studies. Geophys. Res. Lett. 25, 337–340.
Bond, T.C., Streets, D.G., Yarber, K.F., Nelson, S.M., Woo, J.H., Klimont, Z., 2004. A technology-based global inventory of black and organic carbon emissions from combustion. J. Geophys. Res.-Atmos. 109.
Bond, T.C., Doherty, S.J., Fahey, D.W., Forster, P.M., Berntsen, T., DeAngelo, B.J., Flanner, M.G., Ghan, S., Karcher, B., Koch, D., Kinne, S., Kondo, Y., Quinn, P.K., Sarofim, M.C., Schultz, M.G., Schulz, M., Venkataraman, C., Zhang, H., Zhang, S., Bellouin, N., Guttikunda, S.K., Hopke, P.K., Jacobson, M.Z., Kaiser, J.W., Klimont, Z., Lohmann, U., Schwarz, J.P., Shindell, D., Storelvmo, T., Warren, S.G., Zender, C.S., 2013. Bounding the role of black carbon in the climate system: a scientific assessment. J. Geophys. Res.-Atmos. 118, 5380–5552.
Breon, F.M., Colzy, S., 1999. Cloud detection from the spaceborne POLDER instrument and validation against surface synoptic observations. J. Appl. Meteorol. 38, 777–785.
Chen, H., Gu, X., Cheng, T., Li, Z., Yu, T., 2013. The spatial-temporal variations in optical properties of atmosphere aerosols derived from AERONET dataset over China. Meteorog. Atmos. Phys. 122, 65–73.
China, S., Mazzoleni, C., Gorkowski, K., Aiken, A.C., Dubey, M.K., 2013. Morphology and mixing state of individual freshly emitted wildfire carbonaceous particles. Nat. Commun. 4.
China, S., Scarnato, B., Owen, R.C., Zhang, B., Ampadu, M.T., Kumar, S., Dzepina, K., Dziobak, M.P., Fialho, P., Perlinger, J.A., Hueber, J., Helmig, D., Mazzoleni, L.R., Mazzoleni, C., 2015. Morphology and mixing state of aged soot particles at a remote marine free troposphere site: implications for optical properties. Geophys. Res. Lett. 42, 1243–1250.
Chowdhary, J., Cairns, B., Travis, L.D., 2002. Case studies of aerosol retrievals over the ocean from multiangle, multispectral photopolarimetric remote sensing data. J. Atmos. Sci. 59, 383–397.
DeCarlo, P.F., Kimmel, J.R., Trimborn, A., Northway, M.J., Jayne, J.T., Aiken, A.C., Gonin, M., Fuhrer, K., Horvath, T., Docherty, K.S., Worsnop, D.R., Jimenez, J.L., 2006. Field-deployable, high-resolution, time-of-flight aerosol mass spectrometer. Anal. Chem. 78, 8281–8289.
Dey, S., Tripathi, S.N., Singh, R.P., Holben, B.N., 2006. Retrieval of black carbon and specific absorption over Kanpur city, northern India during 2001–2003 using AERONET data. Atmos. Environ. 40, 445–456.
Dubovik, O., 2004. Optimization of Numerical Inversion in Photopolarimetric Remote Sensing. Springer, Netherlands.
Dubovik, O., King, M.D., 2000. A flexible inversion algorithm for retrieval of aerosol optical properties from Sun and sky radiance measurements. J. Geophys. Res.-Atmos. 105, 20673–20696.
Dubovik, O., Holben, B., Eck, T.F., Smirnov, A., Kaufman, Y.J., King, M.D., Tanre, D., Slutsker, I., 2002. Variability of absorption and optical properties of key aerosol types observed in worldwide locations. J. Atmos. Sci. 59, 590–608.
Dubovik, O., Herman, M., Holdak, A., Lapyonok, T., Tanre, D., Deuze, J.L., Ducos, F., Sinyuk, A., Lopatin, A., 2011. Statistically optimized inversion algorithm for enhanced retrieval of aerosol properties from spectral multi-angle polarimetric satellite observations. Atmos. Meas. Tech. 4, 975–1018.
Ebert, M., Inerle-Hof, M., Weinbruch, S., 2002. Environmental scanning electron microscopy as a new technique to determine the hygroscopic behaviour of individual aerosol particles. Atmos. Environ. 36, 5909–5916.
Flanner, M.G., Zender, C.S., Randerson, J.T., Rasch, P.J., 2007. Present-day climate forcing and response from black carbon in snow. J. Geophys. Res.-Atmos. 112.
Fuller, K.A., Malm, W.C., Kreidenweis, S.M., 1999. Effects of mixing on extinction by carbonaceous particles. J. Geophys. Res.-Atmos. 104, 15941–15954.
Ginoux, P., Chin, M., Tegen, I., Prospero, J.M., Holben, B., Dubovik, O., Lin, S.J., 2001. Sources and distributions of dust aerosols simulated with the GOCART model. J. Geophys. Res.-Atmos. 106, 20255–20273.
He, C., Liou, K.N., Takano, Y., Zhang, R., Zamora, M.L., Yang, P., Li, Q., Leung, L.R., 2015. Variation of the radiative properties during black carbon aging: theoretical and experimental intercomparison. Atmos. Chem. Phys. 15, 11967–11980.
Holben, B.N., Eck, T.F., Slutsker, I., Tanre, D., Buis, J., Setzer, A., Vermote, E., Reagan, J., Kaufman, Y., Nakajima, T., 1998. AERONET—a federated instrument network and data archive for aerosol characterization. Remote Sens. Environ. 66, 1–16.
Jackson, J.M., Liu, H.Q., Laszlo, I., Kondragunta, S., Remer, L.A., Huang, J.F., Huang, H.C., 2013. Suomi-NPP VIIRS aerosol algorithms and data products. J. Geophys. Res.-Atmos. 118, 12673–12689.
Jacobson, M.Z., 2001. Strong radiative heating due to the mixing state of black carbon in atmospheric aerosols. Nature 409, 695–697.
Jayne, J.T., Leard, D.C., Zhang, X.F., Davidovits, P., Smith, K.A., Kolb, C.E., Worsnop, D.R., 2000. Development of an aerosol mass spectrometer for size and composition analysis of submicron particles. Aerosol Sci. Technol. 33, 49–70.
Jiao, Z.T., Hill, M.J., Schaaf, C.B., Zhang, H., Wang, Z.S., Li, X.W., 2014. An anisotropic flat index (AFX) to derive BRDF archetypes from MODIS. Remote Sens. Environ. 141, 168–187.
Jimenez, J.L., Jayne, J.T., Shi, Q., Kolb, C.E., Worsnop, D.R., Yourshaw, I., Seinfeld, J.H., Flagan, R.C., Zhang, X.F., Smith, K.A., Morris, J.W., Davidovits, P., 2003. Ambient aerosol sampling using the aerodyne aerosol mass spectrometer. J. Geophys. Res.-Atmos. 108.
Jones, A., Roberts, D.L., Slingo, A., 1994. A climate model study of indirect radiative forcing by anthropogenic sulfate aerosols. Nature 370, 450–453.
Kaufman, Y.J., Wald, A.E., Remer, L.A., Gao, B.C., Li, R.R., Flynn, L., 1997. The MODIS 2.1-mu m channel - correlation with visible reflectance for use in remote sensing of aerosol. IEEE Trans. Geosci. Remote Sens. 35, 1286–1298.
Khlystov, A., Wyers, G.P., Slanina, J., 1995. The steam-jet aerosol collector. Atmos. Environ. 29, 2229–2234.
Koch, D., Schulz, M., Kinne, S., McNaughton, C., Spackman, J.R., Balkanski, Y., Bauer, S., Berntsen, T., Bond, T.C., Boucher, O., Chin, M., Clarke, A., De Luca, N., Dentener, F., Diehl, T., Dubovik, O., Easter, R., Fahey, D.W., Feichter, J., Fillmore, D., Freitag, S., Ghan, S., Ginoux, P., Gong, S., Horowitz, L., Iversen, T., Kirkevag, A., Klimont, Z., Kondo, Y., Krol, M., Liu, X., Miller, R., Montanaro, V., Moteki, N., Myhre, G., Penner, J.E., Perlwitz, J., Pitari, G., Reddy, S., Sahu, L., Sakamoto, H., Schuster, G., Schwarz, J.P., Seland, O., Stier, P., Takegawa, N., Takemura, T., Textor, C., van Aardenne, J.A., Zhao, Y., 2009. Evaluation of black carbon estimations in global aerosol models. Atmos. Chem. Phys. 9, 9001–9026.
Kotchenova, S.Y., Vermote, E.F., 2007. Validation of a vector version of the 6S radiative transfer code for atmospheric correction of satellite data. Part II. Homogeneous Lambertian and anisotropic surfaces. Appl. Opt. 46, 4455–4464.
Koven, C.D., Fung, I., 2006. Inferring dust composition from wavelength-dependent absorption in aerosol robotic network (AERONET) data. J. Geophys. Res.-Atmos. 111.
Lee, J., Kim, J., Song, C.H., Ryu, J.H., Ahn, Y.H., Song, C.K., 2010. Algorithm for retrieval of aerosol optical properties over the ocean from the geostationary ocean color imager. Remote Sens. Environ. 114, 1077–1088.
Lenoble, J., Herman, M., Deuze, J.L., Lafrance, B., Santer, R., Tanre, D., 2007. A successive order of scattering code for solving the vector equation of transfer in the earth's atmosphere with aerosols. J. Quant. Spectrosc. Radiat. Transf. 107, 479–507.
Lesins, G., Chylek, P., Lohmann, U., 2002. A study of internal and external mixing scenarios and its effect on aerosol optical properties and direct radiative forcing. J. Geophys. Res.-Atmos. 107.
Levy, R.C., Mattoo, S., Munchak, L.A., Remer, L.A., Sayer, A.M., Patadia, F., Hsu, N.C., 2013. The collection 6 MODIS aerosol products over land and ocean. Atmos. Meas. Tech. 6, 2989–3034.
Li, X.W., Strahler, A.H., 1992. Geometric-optical bidirectional reflectance modeling of the discrete crown vegetation canopy - effect of crown shape and mutual shadowing. IEEE Trans. Geosci. Remote Sens. 30, 276–292.
Li, Z., Gu, X., Wang, L., Li, D., Xie, Y., Li, K., Dubovik, O., Schuster, G., Goloub, P., Zhang, Y., Li, L., Ma, Y., Xu, H., 2013. Aerosol physical and chemical properties retrieved from ground-based remote sensing measurements during heavy haze days in Beijing winter. Atmos. Chem. Phys. 13, 10171–10183.
Li, B.G., Gasser, T., Ciais, P., Piao, S.L., Tao, S., Balkanski, Y., Hauglustaine, D., Boisier, J.P., Chen, Z., Huang, M.T., Li, L.Z., Li, Y., Liu, H.Y., Liu, J.F., Peng, S.S., Shen, Z.H., Sun, Z.Z., Wang, R., Wang, T., Yin, G.D., Yin, Y., Zeng, H., Zeng, Z.Z., Zhou, F., 2016. The contribution of China's emissions to global climate forcing. Nature 531, 357.
Li, M., Zhang, Q., Kurokawa, J.-i., Woo, J.-H., He, K., Lu, Z., Ohara, T., Song, Y., Streets, D.G., Carmichael, G.R., 2017. MIX: a mosaic Asian anthropogenic emission inventory under the international collaboration framework of the MICS-Asia and HTAP. Atmos. Chem. Phys. 17.
Liousse, C., Cachier, H., Jennings, S.G., 1993. Optical and thermal measurements of black carbon aerosol content in different environments - variation of the specific attenuation cross-section, sigma (sigma). Atmos. Environ. Part A 27, 1203–1211.
Lohmann, U., Feichter, J., 2005. Global indirect aerosol effects: a review. Atmos. Chem. Phys. 5, 715–737.
Mackowski, D.W., Mishchenko, M.I., 2011. A multiple sphere T-matrix Fortran code for use on parallel computer clusters. J. Quant. Spectrosc. Radiat. Transf. 112, 2182–2192.
Martonchik, J.V., Diner, D.J., Kahn, R.A., Ackerman, T.P., Verstraete, M.E., Pinty, B., Gordon, H.R., 1998. Techniques for the retrieval of aerosol properties over land and ocean using multiangle imaging. IEEE Trans. Geosci. Remote Sens. 36, 1212–1227.
Ng, N.L., Herndon, S.C., Trimborn, A., Canagaratna, M.R., Croteau, P.L., Onasch, T.B., Sueper, D., Worsnop, D.R., Zhang, Q., Sun, Y.L., Jayne, J.T., 2011. An aerosol

chemical speciation monitor (ACSM) for routine monitoring of the composition and mass concentrations of ambient aerosol. Aerosol Sci. Technol. 45, 780–794.
Omar, A.H., Won, J.G., Winker, D.M., Yoon, S.C., Dubovik, O., McCormick, M.P., 2005. Development of global aerosol models using cluster analysis of aerosol robotic network (AERONET) measurements. J. Geophys. Res.-Atmos. 110.
Ortega, J.M., Rheinboldt, W.C., 1970. Iterative Solution of Nonlinear Equations in Several Variables. Academic Press.
Ramanathan, V., Carmichael, G., 2008. Global and regional climate changes due to black carbon. Nat. Geosci. 1, 221–227.
Ran, L., Deng, Z.Z., Xu, X.B., Yan, P., Lin, W.L., Wang, Y., Tian, P., Wang, P.C., Pan, W.L., Lu, D.R., 2016. Vertical profiles of black carbon measured by a micro-aethalometer in summer in the North China Plain. Atmos. Chem. Phys. 16, 10441–10454.
Randerson, J.T., Liu, H., Flanner, M.G., Chambers, S.D., Jin, Y., Hess, P.G., Pfister, G., Mack, M.C., Treseder, K.K., Welp, L.R., Chapin, F.S., Harden, J.W., Goulden, M.L., Lyons, E., Neff, J.C., Schuur, E.A.G., Zender, C.S., 2006. The impact of boreal forest fire on climate warming. Science 314, 1130–1132.
Samset, B.H., Myhre, G., 2011. Vertical dependence of black carbon, sulphate and biomass burning aerosol radiative forcing. Geophys. Res. Lett. 38.
Sato, M., Hansen, J., Koch, D., Lacis, A., Ruedy, R., Dubovik, O., Holben, B., Chin, M., Novakov, T., 2003. Global atmospheric black carbon inferred from AERONET. Proc. Natl. Acad. Sci. U. S. A. 100, 6319–6324.
Scarnato, B.V., Vahidinia, S., Richard, D.T., Kirchstetter, T.W., 2013. Effects of internal mixing and aggregate morphology on optical properties of black carbon using a discrete dipole approximation model. Atmos. Chem. Phys. 13, 5089–5101.
Schaaf, C.B., Gao, F., Strahler, A.H., Lucht, W., Li, X.W., Tsang, T., Strugnell, N.C., Zhang, X.Y., Jin, Y.F., Muller, J.P., Lewis, P., Barnsley, M., Hobson, P., Disney, M., Roberts, G., Dunderdale, M., Doll, C., d'Entremont, R.P., Hu, B.X., Liang, S.L., Privette, J.L., Roy, D., 2002. First operational BRDF, albedo nadir reflectance products from MODIS. Remote Sens. Environ. 83, 135–148.
Schuster, G.L., Dubovik, O., Holben, B.N., Clothiaux, E.E., 2005. Inferring black carbon content and specific absorption from aerosol robotic network (AERONET) aerosol retrievals. J. Geophys. Res.-Atmos. 110.
Streets, D.G., Yan, F., Chin, M., Diehl, T., Mahowald, N., Schultz, M., Wild, M., Wu, Y., Yu, C., 2009. Anthropogenic and natural contributions to regional trends in aerosol optical depth, 1980–2006. J. Geophys. Res.-Atmos. 114.
Sun, H.L., Biedermann, L., Bond, T.C., 2007. Color of brown carbon: a model for ultraviolet and visible light absorption by organic carbon aerosol. Geophys. Res. Lett. 34.
Takemura, T., Nozawa, T., Emori, S., Nakajima, T.Y., Nakajima, T., 2005. Simulation of climate response to aerosol direct and indirect effects with aerosol transport-radiation model. J. Geophys. Res.-Atmos. 110.
Torres, B., Dubovik, O., Fuertes, D., Schuster, G., Cachorro, V.E., Lapyonok, T., Goloub, P., Blarel, L., Barreto, A., Mallet, M., Toledano, C., Tanre, D., 2017. Advanced characterisation of aerosol size properties from measurements of spectral optical depth using the GRASP algorithm. Atmos. Meas. Tech. 10, 3743–3781.
van Beelen, A.J., Roelofs, G.J.H., Hasekamp, O.P., Henzing, J.S., Rockmann, T., 2014. Estimation of aerosol water and chemical composition from AERONET Sun-sky radiometer measurements at Cabauw, the Netherlands. Atmos. Chem. Phys. 14, 5969–5987.
Vermote, E.F., Tanre, D., Deuze, J.L., Herman, M., Morcrette, J.J., 1997. Second simulation of the satellite signal in the solar Spectrum, 6S: an overview. IEEE Trans. Geosci. Remote Sens. 35, 675–686.
Wang, L., Li, Z.Q., Li, D.H., Li, K.T., Tian, Q.J., Li, L., Zhang, Y., Lu, Y., Gu, X.F., 2012. Retrieval of dust fraction of atmospheric aerosols based on spectra characteristics of refractive indices obtained from remote sensing measurements. Spectrosc. Spectr. Anal. 32, 1644–1649.
Wang, L., Li, Z.Q., Tian, Q.J., Ma, Y., Zhang, F.X., Zhang, Y., Li, D.H., Li, K.T., Li, L., 2013. Estimate of aerosol absorbing components of black carbon, brown carbon, and dust from ground-based remote sensing data of sun-sky radiometers. J. Geophys. Res.-Atmos. 118, 6534–6543.
Wang, Y.Y., Liu, F.S., He, C.L., Bi, L., Cheng, T.H., Wang, Z.L., Zhang, H., Zhang, X.Y., Shi, Z.B., Li, W.J., 2017. Fractal dimensions and mixing structures of soot particles during atmospheric processing. Environ. Sci. Technol. Lett. 4, 487–493.
Wiscombe, W.J., 1980. Improved Mie scattering algorithms. Appl. Opt. 19, 1505–1509.
Wu, Y., Cheng, T.H., Liu, D.T., Allan, J.D., Zheng, L.J., Chen, H., 2018. Light absorption enhancement of black carbon aerosol constrained by particle morphology. Environ. Sci. Technol. 52, 6912–6919.
Xie, Y.S., Li, Z.Q., Zhang, Y.X., Zhang, Y., Li, D.H., Li, K.T., Xu, H., Zhang, Y., Wang, Y.Q., Chen, X.F., Schauer, J.J., Bergin, M., 2017. Estimation of atmospheric aerosol composition from ground-based remote sensing measurements of Sun-sky radiometer. J. Geophys. Res.-Atmos. 122, 498–518.
Xu, R., Tie, X., Li, G., Zhao, S., Cao, J., Feng, T., Long, X., 2018. Effect of biomass burning on black carbon (BC) in South Asia and Tibetan plateau: the analysis of WRF-Chem modeling. Sci. Total Environ. 645, 901–912.
Yang, Y., Wang, H.L., Smith, S.J., Easter, R., Ma, P.L., Qian, Y., Yu, H.B., Li, C., Rasch, P.J., 2017. Global source attribution of sulfate concentration and direct and indirect radiative forcing. Atmos. Chem. Phys. 17, 8903–8922.